BNL-94458-2010

Neutron Cross section Covariances in the Resonance region: ^{50,53}Cr, ^{54,57}Fe and ^{60}Ni

P.Oblozinsky, Y.-S.Cho[*)], C.M.Mattoon[†)], S.F.Mughabghab

National Nuclear Data Center, Brookhaven National Laboratory

Upton, NY 11793- 5000, USA

*) On sabbatical leave from Nuclear Data Laboratory, KAERI, Korea

[†)] Present address: Lawrence Livermore National Laboratory, Livermore, California, U.S.A.

November 23, 2010

National Nuclear Data Center
Brookhaven National Laboratory
P.O. Box 5000
Upton, NY 11973-5000
www.nndc.bnl.gov

Notice: This manuscript has been authored by employees of Brookhaven Science Associates, LLC under Contract No. DE-AC02-98CH10886 with the U.S. Department of Energy. The publisher by accepting the manuscript for publication acknowledges that the United States Government retains a non-exclusive, paid-up, irrevocable, world-wide license to publish or reproduce the published form of this manuscript, or allow others to do so, for United States Government purposes.

DISCLAIMER

This report was prepared as an account of work sponsored by an agency of the United States Government. Neither the United States Government nor any agency thereof, nor any of their employees, nor any of their contractors, subcontractors, or their employees, makes any warranty, express or implied, or assumes any legal liability or responsibility for the accuracy, completeness, or any third party's use or the results of such use of any information, apparatus, product, or process disclosed, or represents that its use would not infringe privately owned rights. Reference herein to any specific commercial product, process, or service by trade name, trademark, manufacturer, or otherwise, does not necessarily constitute or imply its endorsement, recommendation, or favoring by the United States Government or any agency thereof or its contractors or subcontractors. The views and opinions of authors expressed herein do not necessarily state or reflect those of the United States Government or any agency thereof..

Neutron cross section covariances in the resonance region: ^{50,53}Cr, ^{54,57}Fe and ^{60}Ni

P. Obložinský, Y.-S. Cho*), C.M. Mattoon†), S.F. Mughabghab

National Nuclear Data Center, Brookhaven National Laboratory
Upton, New York, 11973 – 5000, U.S.A.

*) On sabbatical leave from Nuclear Data Lab, KAERI, Korea

†) Present address: Lawrence Livermore National Laboratory, Livermore, California, U.S.A.

November 23, 2010

Notice: This manuscript has been authored by employees of Brookhaven Science Associates, LLC under Contract No. DE-AC02-98CH10886 with the U.S. Department of Energy. The publisher by accepting the manuscript for publication acknowledges that the United States Government retains a non-exclusive, paid-up, irrevocable, world-wide license to publish or reproduce the published form of this manuscript, or allow others to do so, for United States Government purposes.

Abstract

We evaluated covariances in the neutron resonance region for capture and elastic scattering cross sections on minor structural materials, ^{50,53}Cr, ^{54,57}Fe and ^{60}Ni. Use was made of the recently developed covariance formalism based on kernel approximation along with data in the Atlas of Neutron Resonances. Our results of most interest for advanced fuel cycle applications, elastic scattering cross section uncertainties at energies around 100 keV, are on the level of about 7-10%.

Contents

1 Introduction **2**

2 Evaluation procedure **3**
2.1 Radiative capture 3
2.1.1 Thermal region 3
2.1.2 Resonance region 4
2.2 Elastic scattering 6
2.2.1 Thermal region 6
2.2.2 Resonance region - average cross sections 7
2.2.3 Resonance region - uncertainties 8
2.2.4 Resonance region - covariance matrix 9

3 Evaluations **11**
3.1 Input uncertainties 11
3.1.1 Resonance parameter uncertainties 11
3.1.2 Integral uncertainties - capture 12
3.1.3 Integral uncertainties - elastic 14
3.2 ^{50}Cr evaluation 16
3.2.1 Capture 17
3.2.2 Elastic 20
3.3 ^{53}Cr evaluation 24
3.3.1 Capture 25
3.3.2 Elastic 28
3.4 ^{54}Fe evaluation 32
3.4.1 Capture 33
3.4.2 Elastic 36
3.5 ^{57}Fe evaluation 40
3.5.1 Capture 41

3.5.2 Elastic 44
3.6 ^{60}Ni evaluation 48
3.6.1 Capture 49
3.6.2 Elastic 52

4 Quality assurance **56**
4.1 Compliance with ENDF-6 format 56
4.2 Mathematical properties of covariance matrices 56
4.3 Cross section uncertainties 57
4.3.1 Capture 57
4.3.2 Elastic scattering 60
4.3.3 Minimal uncertainties 61

5 Conclusions **62**

Bibliography **64**

Chapter 1

Introduction

This report describes evaluation/estimate of covariances of neutron capture and neutron elastic scattering cross sections in the resonance region for five minor structural materials in the Cr-Fe-Ni mass range, ^{50,53}Cr, ^{54,57}Fe and ^{60}Ni. The report complements our earlier work on covariances for three major structural materials, ^{52}Cr, ^{56}Fe and ^{58}Ni [1]. In both instances we used our new covariance formalism based on kernel approximation described in Ref. [2] with refinements described in Ref. [1].

Produced covariances should be incorporated into improved AFCI covariance library, AFCI-2.0, which is under development by BNL-LANL collaboration for Advanced Fuel Cycle Initiative applications [3]. This library is supplied in 33-energy group representation, covering energies from 19.66 MeV down to 10^{-5} eV in nearly uniform (near-constant lethargy) energy groups. We emphasize that the kernel approximation produces covariances averaged over relatively broad energy bins, which should be well suited for AFCI applications.

The report is organized as follows. In Chapter 2 we summarize adopted formalism, which is followed by Chapter 3 where we describe results of evaluation for individual materials. Chapter 4 is devoted to quality assurance and conclusions are drawn in Chapter 5.

Chapter 2

Evaluation procedure

Detailed description of adopted evaluation procedure can be found in Ref. [2]. Its key idea is the use of kernel approximation which allowed us to develop analytical formalism of propagating resonance parameter uncertainties from Atlas of Neutron Resonances [4] into cross sections uncertainties. Refinements of the evaluation procedure are described in the report devoted to evaluation of three major structural materials, ^{52}Cr, ^{56}Fe and ^{58}Ni [1]. Brief summary of the evaluation procedure is given below for convenience.

2.1 Radiative capture

Covariances in thermal and resonance regions are treated separately. In the thermal region we use experimentally determined uncertainties of integral quantities. In the resonance region we use kernel approximation.

2.1.1 Thermal region

In the thermal region capture cross sections in general follow the well-known 1/v law. The upper energy limit for applicability of this law for Cr-Fe-Ni extends up to few hundred eV, depending on the position of the first resonance. In the energy range below 0.5 eV we use experimentally determined uncertainty of the thermal cross section, $\Delta\sigma(E_{th})$. At higher energies of the thermal region, 0.5 eV-1 keV for materials discussed here, we adopt experimentally determined uncertainty of

capture resonance integral, ΔRI_γ. Thus,

$$\Delta\sigma_\gamma(E) = \begin{cases} \Delta\sigma_\gamma(E_{th}) & \text{if } E < 0.5\ eV, \\ \Delta RI_\gamma & \text{if } 0.5\ eV < E \lesssim 1\ keV. \end{cases} \tag{2.1}$$

This choice guarantees good agreement with uncertainties of both thermal cross sections and resonance integrals given in Atlas of Neutron Resonances.

2.1.2 Resonance region

Kernel approximation is used in the resonance region. We proceed in three steps, first establish suitable energy bins and determine average cross sections, then compute uncertainties of these average cross sections for each bin, and finally combine bin uncertainties into covariance matrix. One can either use capture kernel values directly available in Atlas or compute them from resonance parameters or combination of the two.

Within the single-level Breit-Wigner (SLBW) formalism for an isolated resonance of the energy E_0 located in sufficiently broad bin with the energy width $\Delta E = E_1 - E_2$ the average capture cross section can be expressed as

$$\bar{\sigma}_\gamma = \frac{1}{\Delta E}\int_{E_2}^{E_1} \sigma_\gamma(E)dE \approx a\frac{g\Gamma_n\Gamma_\gamma}{\Gamma}\,, \tag{2.2}$$

where

$$a = 4.089 \times 10^6 \frac{(A+1)^2}{A^2}\frac{1}{E_0\Delta E} \tag{2.3}$$

is given in units of barn/eV and

$$A_\gamma = \frac{g\Gamma_n\Gamma_\gamma}{\Gamma} \tag{2.4}$$

is the capture kernel given in eV. Here, g is the statistical spin factor $g = (2J + 1)/2(2I+2)$, J being the spin of the resonance and I the spin of the target nucleus; Γ_n, Γ_γ and Γ are the neutron, radiative and total width, respectively. We note that up to some fluctuations the average capture cross section is decreasing with the incident neutron energy due to $1/E_0$ term in Eq. (2.3).

The relative uncertainty (standard deviation) of the average capture cross section for a single resonance can be obtained from kernel as

$$\Delta\bar{\sigma}_\gamma = \frac{\delta\bar{\sigma}_\gamma}{\sigma_\gamma} = \frac{\delta A_\gamma}{A_\gamma} = \Delta A_\gamma \,. \tag{2.5}$$

This is convenient if kernel uncertainty can be taken directly from Atlas. If kernel is computed from resonance parameters, then somewhat more involved procedure is needed to propagate resonance parameter uncertainties into kernel uncertainty and thus to average capture cross section [2].

If several resonances are combined together into one energy bin one computes uncertainty from the binomial expression for quadratic summation of uncertainties,

$$(\Delta\bar{\sigma}_\gamma)^2 = \langle \Delta\bar{\sigma}_\gamma \, \Delta\bar{\sigma}_\gamma \rangle = \left\langle \sum_i \Delta A_{\gamma i} \times \sum_r \Delta A_{\gamma r} \right\rangle , \tag{2.6}$$

where $(\Delta\bar{\sigma}_\gamma)^2$ is the variance for a given energy bin, and i and r stand for individual resonances. This yields

$$(\Delta\bar{\sigma}_\gamma)^2 = \sum_i \left(\Delta A_{\gamma i}\right)^2 + 2 \sum_{i,r} \Delta A_{\gamma i} \left\langle \Delta A_{\gamma i} \, \Delta A_{\gamma r} \right\rangle \Delta A_{\gamma r} \,, \tag{2.7}$$

where $\left\langle \Delta A_{\gamma i} \, \Delta A_{\gamma r} \right\rangle$ is the resonance-resonance correlation coefficient. In accordance with Ref.[2] our default values for these coefficients for each energy bin are uniformly set to

$$\mathrm{corr}(A_{\gamma i}, A_{\gamma r}) = \left\langle \Delta A_{\gamma i} \Delta A_{\gamma r} \right\rangle = 0.5. \tag{2.8}$$

Covariance matrix is composed of the thermal and resonance components. The covariance in the thermal region is self-correlated, with just two diagonal terms. In the resonance region the diagonal terms of the covariance matrix are given by the variances of average capture cross sections in chosen energy bins, while the off-diagonal terms represent bin-bin correlations. As no information on correlations is available in Atlas, correlation coefficients must be estimated following certain basic principles. In accordance with Eq. (2.8) our default values were set to 0.5.

Under these assumptions the correlation matrix is composed of two blocks, one corresponds to fully correlated thermal region and another one to the resonance region with off-diagonal terms equal to 0.5. The diagonal terms are always

equal to 1, two blocks are uncorrelated (zeros are replaced by blanks). Thus, the covariance matrix has the form

$$\begin{pmatrix} (\Delta\sigma_\gamma(E_{\rm th}))^2 \\ (\Delta RI_\gamma)^2 \\ (\Delta\bar{\sigma}_{\gamma,1})^2 \\ (\Delta\bar{\sigma}_{\gamma,2})^2 \\ (\Delta\bar{\sigma}_{\gamma,3})^2 \\ \vdots \end{pmatrix} \begin{pmatrix} 1 & 1 & & & & \\ 1 & 1 & & & & \\ & & 1 & 0.5 & 0.5 & \dots \\ & & 0.5 & 1 & 0.5 & \dots \\ & & 0.5 & 0.5 & 1 & \dots \\ & & \vdots & \vdots & \vdots & \ddots \end{pmatrix} \tag{2.9}$$

2.2 Elastic scattering

Similar to capture, covariances for neutron elastic scattering in the thermal and resonance regions are treated separately.

2.2.1 Thermal region

Elastic scattering cross sections are approximately constant over a large portion of the thermal energy range. For materials under discussion this extends up to 100 eV or so. At sub-thermal energies, under the free-gas approximation, this constant behavior changes to 1/v due to molecular motion of target nuclei.

In accordance with the procedure adopted by the low-fidelity covariance project [5], in the energy range below 0.5 eV we adopt uncertainty of thermal free-atom nuclear elastic cross section. An assumption that at energies above 0.5 eV one can still resort to the same relative uncertainty, often adopted by the low-fidelity project, can be challenged and we adopted more conservative approach. Thus, relative scattering cross section uncertainty in the thermal region is estimated as

$$\Delta\sigma_n(E) = \begin{cases} \Delta\sigma_n(E_{th}) & \text{if } 10^{-3}\ eV < E < 0.5\ eV, \\ 1.5 \cdot \Delta\sigma_n(E_{th}) & \text{if } 0.5\ eV < E \lesssim 100\ eV, \end{cases} \tag{2.10}$$

where $\sigma_n(E_{th}) = \sigma_s$ is the free thermal scattering cross section, which in most cases is directly given in Atlas of Neutron Resonances.*

*Atlas uses notation σ_s for free neutron scattering cross sections.

2.2.2 Resonance region - average cross sections

Following ENDF-6 Formats Manual [6] neutron elastic scattering cross section in SLBW representation can be expressed as

$$\sigma_n(E) = 4\pi\lambda\!\!\!^{-2}(2l+1)\sin^2\phi_l + \pi\lambda\!\!\!^{-2} g \frac{\Gamma_n^2 - 2\Gamma_n\Gamma\sin^2\phi_l + 2(E-E_0)\Gamma_n\sin(2\phi_l)}{(E-E_0)^2 + \frac{1}{4}\Gamma^2}, \tag{2.11}$$

where $\lambda\!\!\!^{-}$ is the incident neutron wave length (alternatively often used wave number is defined as $k = 1/\lambda\!\!\!^{-}$) and ϕ_l is the phase shift,

$$\phi_l = \begin{cases} kR' & \text{if } l = 0 \\ kR' - \arctan(kR') & \text{if } l = 1 \\ kR' - \arctan(3kR'/(3-(kR')^2) & \text{if } l = 2, \end{cases} \tag{2.12}$$

where R' is the scattering radius.

The average scattering cross section in sufficiently broad energy bin of the width $\Delta E = E_1 - E_2$ around the resonance energy E_0 can be obtained as

$$\bar{\sigma}_n = \frac{1}{E_2 - E_1}\int_{E_1}^{E_2} \sigma_n(E)dE = \bar{\sigma}_n^{pot} + \bar{\sigma}_n^{res}, \tag{2.13}$$

where the average potential scattering cross section

$$\bar{\sigma}_n^{pot} \approx 4\pi\lambda\!\!\!^{-2}(2l+1)\sin^2\phi_l\,, \tag{2.14}$$

and the average resonance scattering cross section

$$\bar{\sigma}_n^{res} \approx a\frac{g\Gamma_n(\Gamma_n - 2\Gamma\sin^2\phi_l)}{\Gamma}, \tag{2.15}$$

with $\sin^2\phi_l$ computed at E_0.

We note that while $\bar{\sigma}_n^{pot}$ is slowly decreasing with energy, the resonance term has $1/E_0$ dependence and $\bar{\sigma}_n^{res}$ vanishes with the energy. Therefore, if resonances extend to hundreds of keV as is the case for structural materials, neutron elastic scattering is determined by potential scattering. Consequently, elastic scattering uncertainties are driven by $\Delta R'$ rather than resonance parameter uncertainties.

2.2.3 Resonance region - uncertainties

Relative uncertainty of the average elastic scattering cross section is obtained by quadratic summation of the resonance and potential scattering terms, $\Delta\bar{\sigma}_n^{res}$ and $\Delta\bar{\sigma}_n^{pot}$. The outcome depends on the correlation between these two terms, our default value being

$$\langle \Delta\bar{\sigma}_n^{res} \Delta\bar{\sigma}_n^{pot} \rangle = -0.5. \tag{2.16}$$

Uncertainty of the resonance term is determined from sensitivities of the average elastic resonance scattering cross section, $\bar{\sigma}_n^{res}$, to Γ_n, Γ_γ and R', followed by quadratic summation,

$$\langle \delta\bar{\sigma}_n^{res} \rangle^2 = \left\langle \frac{\partial\bar{\sigma}_n^{res}}{\partial\Gamma_n}\delta\Gamma_n + \frac{\partial\bar{\sigma}_n^{res}}{\partial\Gamma_n}\delta\Gamma_\gamma + \frac{\partial\bar{\sigma}_n^{res}}{\partial R'}\delta R' \right\rangle^2 . \tag{2.17}$$

Materials in Cr-Fe-Ni mass range are almost pure scatterers,

$$\Gamma_n >> \Gamma_\gamma \quad \text{implying} \quad \delta\Gamma_n >> \delta\Gamma_\gamma . \tag{2.18}$$

Hence the term containing $\delta\Gamma_\gamma$ in Eq. (2.17) can be neglected and

$$\langle \Delta\bar{\sigma}_n^{res} \rangle^2 \approx \left(\frac{\partial\bar{\sigma}_n^{res}}{\partial\Gamma_n}\frac{\delta\Gamma_n}{\bar{\sigma}_n^{res}} \right)^2 + \left(\frac{\partial\bar{\sigma}_n^{res}}{\partial R'}\frac{\delta R'}{\bar{\sigma}_n^{res}} \right)^2 + 2\frac{\partial\bar{\sigma}_n^{res}}{\partial\Gamma_n} \left\langle \frac{\delta\Gamma_n \delta R'}{\bar{\sigma}_n^{res}\bar{\sigma}_n^{res}} \right\rangle \frac{\partial\bar{\sigma}_n^{res}}{\partial R'} . \tag{2.19}$$

The 1st term in Eq. (2.19) can be approximated for small ϕ_l as

$$\frac{\partial\bar{\sigma}_n^{res}}{\partial\Gamma_n}\frac{\delta\Gamma_n}{\bar{\sigma}_n^{res}} \approx \frac{\delta\Gamma_n}{\Gamma_n} = \Delta\Gamma_n, \tag{2.20}$$

the 2nd term as

$$\frac{\partial\bar{\sigma}_n^{res}}{\partial R'}\frac{\delta R'}{\bar{\sigma}_n^{res}} \approx \frac{4\sin\phi_l\cos\phi_l}{1-2\sin^2\phi_l} k\Delta R' , \tag{2.21}$$

and the 3rd term can be easily obtained from the first two once anti-correlation between Γ_n and R' has been properly estimated.

Uncertainty of the potential term is obtained from potential scattering by summing up s-waves and p-waves (d-waves can be neglected) and distant level contributions,

$$\sigma_n^{pot}(E) = \frac{4\pi}{k^2}\left\{ \sin^2(kR') + 3\sin^2\left[(kR') - \arctan(kR')\right] \right\} . \tag{2.22}$$

As shown in Ref. [2] one can compute sensitivities analytically and obtain uncertainty of potential scattering cross section as

$$\Delta\bar{\sigma}_n^{pot} = \frac{\partial\bar{\sigma}_n^{pot}}{\partial R'}\frac{\delta R'}{\bar{\sigma}_n^{pot}} = 2\Delta R'\left\{kR'\frac{sin\phi_0\cos\phi_0 + 3\left(1-\frac{1}{1+(kR')^2}\right)\sin\phi_1\cos\phi_1}{\sin^2\phi_0 + 3\cos^2\phi_1}\right\}, \tag{2.23}$$

where $\Delta R' = \delta R'/R'$ is R' relative uncertainty. Leading term is $2\Delta R'$, term in complex brackets being correction factor which is close to 1 and decreases slowly with energy. As an example, for ^{56}Fe this correction reaches value of 0.9 at 800 keV [2].

Using explicit expressions for the sensitivities and making appropriate assumptions about the correlations between the resonance parameter uncertainties one can get the uncertainty of the average cross section in a given energy bin.

2.2.4 Resonance region - covariance matrix

The last step is combining bin uncertainties into covariance matrix, which is composed of the thermal and resonance components. The thermal region is fully correlated, with two diagonal terms. In the resonance region the diagonal terms are given by the uncertainties of average scattering cross sections in chosen energy bins, while the off-diagonal terms are bin-bin correlation coefficients. Default values of these coefficients are given in Table 2.1; actual values should be determined by an evaluator keeping in mind that no information is available in Atlas of Neutron Resonances.

Elastic scattering correlation matrix is composed of two blocks, one corresponds to fully correlated thermal region and another one to the resonance region with off-diagonal terms equal to 0.5. The diagonal terms are always equal to 1, two blocks are uncorrelated (zeros are replaced by blanks). Thus, the covariance matrix has the form,

$$\begin{pmatrix} (\Delta\sigma_n(E_{\text{th}}))^2 \\ (1.5\Delta\sigma_(E_{\text{th}}))^2 \\ (\Delta\bar{\sigma}_{n,1})^2 \\ (\Delta\bar{\sigma}_{n,2})^2 \\ (\Delta\bar{\sigma}_{n,3})^2 \\ \vdots \end{pmatrix}\begin{pmatrix} 1 & 1 & & & & \\ 1 & 1 & & & & \\ & & 1 & 0.5 & 0.5 & \dots \\ & & 0.5 & 1 & 0.5 & \dots \\ & & 0.5 & 0.5 & 1 & \dots \\ & & \vdots & \vdots & \vdots & \ddots \end{pmatrix} \tag{2.24}$$

Table 2.1: Default values of correlation coefficients (range -1.0 to +1.0) adopted in the present work.

No.	Type	Quantity	Default
1	Single resonance	corr(Γ_n, Γ_γ)	0.0$^{+)}$
2	Resonance-resonance	corr($\Gamma_\gamma, \Gamma_\gamma$)	0.5
3	Resonance-resonance	corr(Γ_n, Γ_n)	0.5
4	Resonance-resonance	corr(Γ_n, Γ_γ)	0.0
5	Pot. scattering-resonance	corr(R', Γ_n)	-0.5
6	Bin-bin	corr($\bar{\sigma}_\gamma, \bar{\sigma}_\gamma$)	0.5
7	Bin-bin	corr($\bar{\sigma}_n, \bar{\sigma}_n$)	0.5
8	Thermal-resonance	corr($\sigma_\gamma^{th}, \bar{\sigma}_\gamma$)	0.0
9	Thermal-resonance	corr($\sigma_n^{th}, \bar{\sigma}_n$)	0.0
10	Cross-correlation	corr($\sigma_n^{th}, \sigma_\gamma^{th}$)	0.0
11	Cross-correlation	corr($\sigma_n^{res}, \sigma_\gamma^{res}$)	0.0$^{\dagger)}$

$^{+)}$ For scattering resonances this could be as large as +0.7 if no correction was carried out by measurer. In analysis by the area method a measurer assumes a value of Γ_γ to obtain Γ_n and for reasonably thick samples (*i.e.*, non-thin) Γ_n is anticorrelated with Γ_γ.
$^{\dagger)}$ This correlation should have little impact except for the thermal region; 0.0 value was adopted for simplicity.

Chapter 3

Evaluations

3.1 Input uncertainties

3.1.1 Resonance parameter uncertainties

Resonance parameter uncertainties for 5 minor structural materials used in the present work were taken from electronic version of Atlas of Neutron Resonances [4]. Availability of these data is summarized in Table 3.1.

Table 3.1: Availability of resonance parameter uncertainties in Atlas for 5 minor structural materials. Maximum resonance energies, $E_0^{\max}$, show availability of $\Delta\Gamma_n, \Delta\Gamma_\gamma$ and ΔA_γ. At higher energies the average radiative widths with uncertainties $\langle\Delta\Gamma_{\gamma 0}\rangle$ and $\langle\Delta\Gamma_{\gamma 1}\rangle$ are usually available.

Nucleus	$E_0^{\max}$	$\Delta\Gamma_n$	$\Delta\Gamma_\gamma$	ΔA_γ	$\langle\Delta\Gamma_{\gamma 0}\rangle$	$\langle\Delta\Gamma_{\gamma 1}\rangle$	Comment
	keV	$E_0^{\max}$	$E_0^{\max}$	$E_0^{\max}$	%	%	
^{50}Cr	591	472	292	297	50	31	$\langle\Delta\Gamma_{\gamma 0}\rangle$ estimated
^{53}Cr	264	244	264	200	50	33	$\langle\Delta\Gamma_{\gamma 0}\rangle$ estimated
^{54}Fe	807	807	195	195	50	26	$\langle\Delta\Gamma_{\gamma 0}\rangle$ estimated
^{57}Fe	190	190	190	190	60	86	
^{60}Ni	451	451	445	451	31	6	

3.1.2 Integral uncertainties - capture

Relative standard deviations (relative uncertainties) for capture integral quantities are summarized in Table 3.2. These quantities include thermal cross sections, resonance integrals and 30-keV Maxwellian averages. Shown are also central values in ENDF/B-VII.0, Atlas, and 30-keV Maxwellian averages in the KADoNis database [7]. Adopted uncertainties for thermal cross sections and resonance integrals served as input in the thermal energy range in accordance with Eq. (2.1). These quantities along with 30-keV Maxwellian averages served also for quality assurance purposes discussed in Chapter 4, p. 56.

Adopted uncertainties of capture integral quantities were determined by the procedure developed by the low-fidelity covariance project [5]. The goal there was to apply adopted integral uncertainties to the differential data in the corresponding energy range. It is understood that ENDF/B-VII.0 cross sections are obtained from resonance parameters which were deduced from measurements of differential data. On the other hand, relevant cross section uncertainties in Atlas were obtained from experiments of integral quantities. Thus, if central value in ENDF/B-VII.0 agrees with Atlas within two absolute standard deviations, then estimated relative standard deviation is

$$\Delta\sigma = \Delta\sigma_{\text{Atlas}} \quad \text{if} \quad |\sigma_{\text{ENDF}} - \sigma_{\text{Atlas}}| < 2\delta\sigma_{\text{Atlas}}. \tag{3.1}$$

If the two central values are discrepant, then adopted relative standard deviation is defined as half the difference between these two central values relative to the average central value,

$$\Delta\sigma = \frac{|\sigma_{\text{ENDF}} - \sigma_{\text{Atlas}}|}{\sigma_{\text{ENDF}} + \sigma_{\text{Atlas}}} \quad \text{if} \quad |\sigma_{\text{ENDF}} - \sigma_{\text{Atlas}}| > 2\delta\sigma_{\text{Atlas}}. \tag{3.2}$$

The logic behind Eq. (3.2) is as follows [8]*. Since the two central values are discrepant and we do not know which one is better, we assume that their average,

$$\frac{\sigma_{\text{ENDF}} + \sigma_{\text{Atlas}}}{2},$$

is the best-estimate value. Next, we assume that the two initial central values lie within two standard deviations of the best-estimate value. This is achieved by

*We are indebted to Mark Williams and Goran Arbanas (ORNL) for illuminating discussion of this topic.

Table 3.2: Capture integral quantities (thermal cross sections, $\sigma_\gamma(E_{th})$; resonance integrals, RI_γ; 30-keV Maxwellian averages, MACS) and their uncertainties for 5 minor structural materials. Data were retrieved from ENDF/B-VII.0, Atlas and KADoNis [7]. Uncertainties adopted by the low-fidelity project are compared with present estimates. For ^{50}Cr and ^{53}Cr present ΔRI_γ estimates differ considerably from our initial values based purely on uncertainties given in Atlas.

Nuc-leus	Quantity	VII.0 +) b	A t l a s b	%	Lowfi *) %	Present %	Note
^{50}Cr	$\sigma_\gamma(E_{th})$	15.9	15.4±0.2	1.3	1.7	2.0	
	RI_γ	7.48	11.7±0.2	1.7	22.1	22	Initial value 4%
	MACS	37.8mb	49±12mb	24	-	24	KADoNiS:49±13mb
^{53}Cr	$\sigma_\gamma(E_{th})$	18.1	18.6±0.6	3.2	3.3	3.3	ENDF/A: 18.09±0.42b
	RI_γ	8.43	12.3^c	-	18.7	19	Initial value 6.6%
	MACS	31.4mb	54±9.4mb	17	-	27	KADoNiS:58±10mb
^{54}Fe	$\sigma_\gamma(E_{th})$	2.25	2.25±0.18	8.0	8.0	8.0	
	RI_γ	1.20	1.27±0.10^c	7.9	8.1	8.0	Initial value 7.9%
	MACS	21.6mb	34±3mb	9	-	22	KADoNiS:29.6±1.3mb
^{57}Fe	$\sigma_\gamma(E_{th})$	2.43	2.48±0.30	12	12.2	12	
	RI_γ	1.45	1.52±0.15^c	9.9	10.1	10	Initial value 9.9%
	MACS	28.5mb	-	-	-	18	KADoNiS:40±4mb
^{60}Ni	$\sigma_\gamma(E_{th})$	2.76	2.50±0.06	2.4	5.0	5.0	ENDF/A: 2.40±0.06b
	RI_γ	1.40	1.40±0.20^c	14	14.3	14	Initial value 14%
	MACS	28.3mb	-	-	-	3	KADoNiS:29.9±0.7mb

+) Retrieved from www.nndc.bnl.gov/sigma at 300K (August, 2010).

*) Retrieved from www.nndc.bnl.gov/lowfi (August, 2010).

^{c} Value in Atlas is computed.

defining their difference accordingly, meaning that half their difference,

$$\frac{|\sigma_{\text{ENDF}} - \sigma_{\text{Atlas}}|}{2},$$

is the standard deviation of the best-estimate value. Then, similar to Eq. (3.1), the relative uncertainty of the best-estimate integral quantity is adopted as the relative uncertainty of ENDF/B-VII.0 cross sections.

One may argue, however, that $\Delta\sigma$ should be computed relative to σ_{ENDF} rather than to $(\sigma_{\text{ENDF}}+\sigma_{\text{Atlas}})/2$. The trouble is that the former has some unfortunate features, such as yielding values in considerable excess of 100% if $\sigma_{\text{ENDF}} << \sigma_{\text{Atlas}}$. On the other hand, Eq. (3.2) guarantees that 100% maximum is not exceeded. In addition, it also provides for smooth change when going from consistent data to discrepant data. Since any attempt to resolve the issue of discrepant data without detailed analysis is virtually impossible, we followed the procedure outlined above.

3.1.3 Integral uncertainties - elastic

Relative standard deviations (relative uncertainties) for elastic scattering integral quantities are summarized in Table 3.3. They include three quantities: thermal cross sections, $\sigma_n(E_{\text{th}})$; values in the thermal region at higher energies, $\sigma_n(E > 0.5eV)$; and scattering radii R'. Adopted uncertainties in the thermal energy range were used as input according to Eq. (2.10).

In addition, we also need $\Delta R'$ in the resonance region. The trouble is that the values given in Atlas which are shown in Table 3.3 refer to the thermal region. In order to account for considerable difference in the thermal and resonance energies and possible implications for $\Delta R'$ in the resonance region, we adopted values enhanced by appropriate factor compared to thermal values,

$$\Delta R'(E_{\text{res}}) \approx k_{R'}\Delta R'(E_{\text{th}}), \tag{3.3}$$

where E_{res} stands for the energy in the resonance region. The enhancement factor was initially estimated as $k_{R'} = 2$ [1], in the present work we used

$$k_{R'} = 1.5. \tag{3.4}$$

Table 3.3: Elastic scattering cross sections (in barns) in the thermal region and their uncertainties for 5 minor structural materials. Also given are values of scattering radius, R' (in fm) and $\Delta R'$. Shown are absolute values in ENDF/B-VII.0 and Atlas; uncertainties in Atlas, low-fidelity project, and values adopted in the present work.

Nuc-leus	Quantity	VII.0*	A t l a s		Lowfi†	Present	Note
		b or *fm*	*b* or *fm*	%	%	%	
^{50}Cr	$\sigma_n(E_{th})$	2.37	2.41±0.06	2.5	-	2.5	
	$\sigma_n(E > 0.5eV)$				-	3.7	Estimated
	R'	5.37	5.0±0.3	6.0	-	9.0	$k_{R'}$=1.5
^{53}Cr	$\sigma_n(E_{th})$	7.92	7.76±0.20	2.6	2.6	2.6	ENDF/A: 7.98±0.28
	$\sigma_n(E > 0.5eV)$				2.6	3.9	Estimated
	R'	5.48	5.4±0.3	5.6	-	8.3	$k_{R'}$=1.5
^{54}Fe	$\sigma_n(E_{th})$	2.20	2.17±0.10	4.6	4.6	4.6	
	$\sigma_n(E > 0.5eV)$				4.6	6.9	Estimated
	R'	5.48	5.0	-	-	6.0	Estimated
^{57}Fe	$\sigma_n(E_{th})$	2.62	0.68±0.06	8.8	58	50	
	$\sigma_n(E > 0.5eV)$				58	50	Estimated
	R'	5.90	6.1	-	-	6.0	Estimated
^{60}Ni	$\sigma_n(E_{th})$	0.98	0.98±0.07	7.1	7.2	7.1	ENDF/A: 1.10±0.03
	$\sigma_n(E > 0.5eV)$				7.2	11	Estimated
	R'	6.0	6.7±0.3	4.5	-	6.0	Estimated

*) ENDF/B-VII.0 values retrieved from www.nndc.bnl.gov/sigma (July, 2010).

†) Lowfi values retrieved from www.nndc.bnl.gov/lowfi (July, 2010).

3.2 ^{50}Cr evaluation

Evaluation is performed in several consecutive steps. We start with inspecting capture and elastic scattering cross sections in ENDF/B-VII.0 library. Then, we identify the proper energy binning for average cross sections, compute uncertainties of the average cross sections in these energy bins, and finally combine the bins into covariance matrix. Details can be seen on subsequent plots.

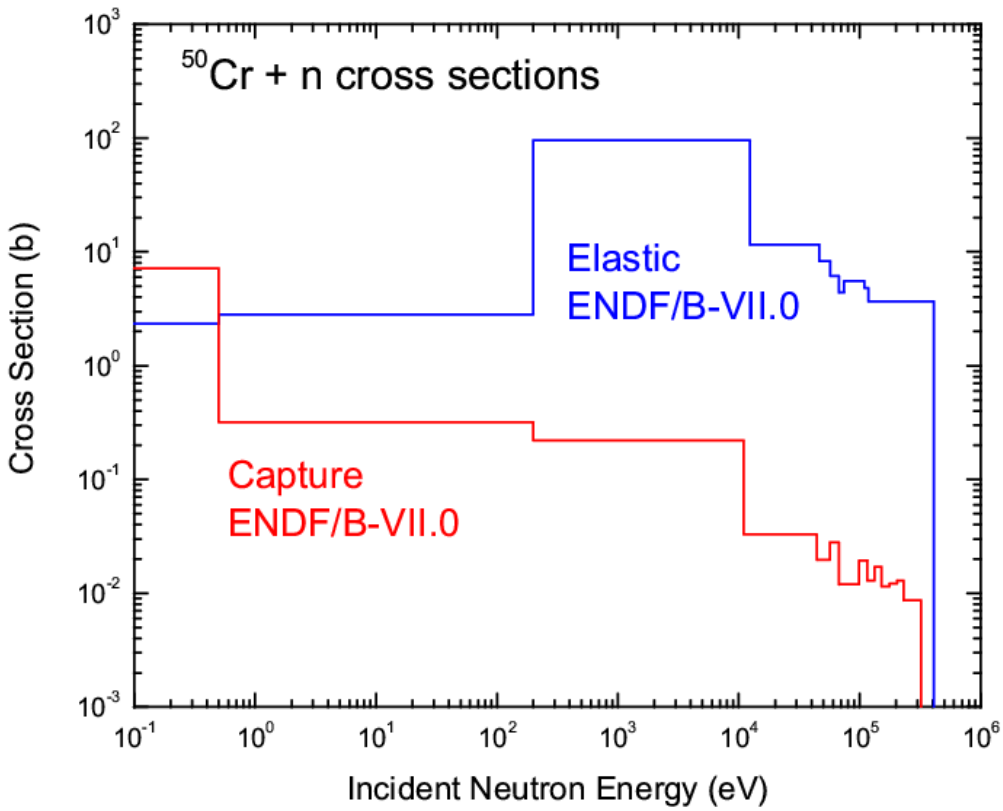

Figure 3.1: ^{50}Cr(n,γ) and (n,el) average cross sections in the thermal and resonance region using resonance parameters from ENDF/B-VII.0 processed by NJOY.

3.2.1 Capture

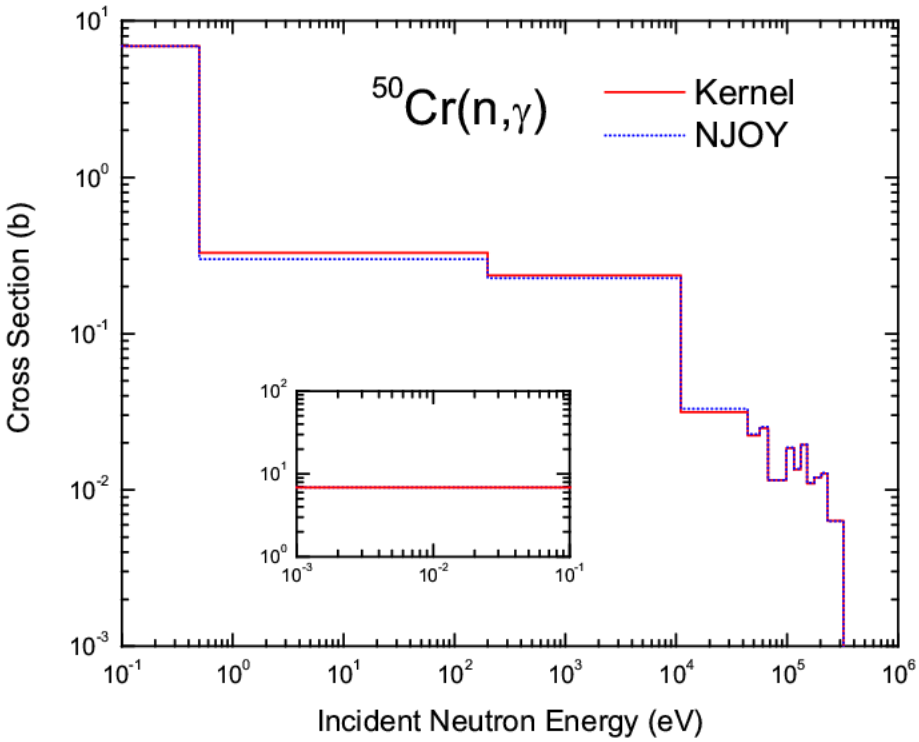

Figure 3.2: ^{50}Cr(n,γ) average cross sections using resonance parameters from Atlas. Compared are approximate values obtained by kernel formalism with correct values obtained by NJOY, demonstrating an excellent agreement. Shown in the insert is the thermal region.

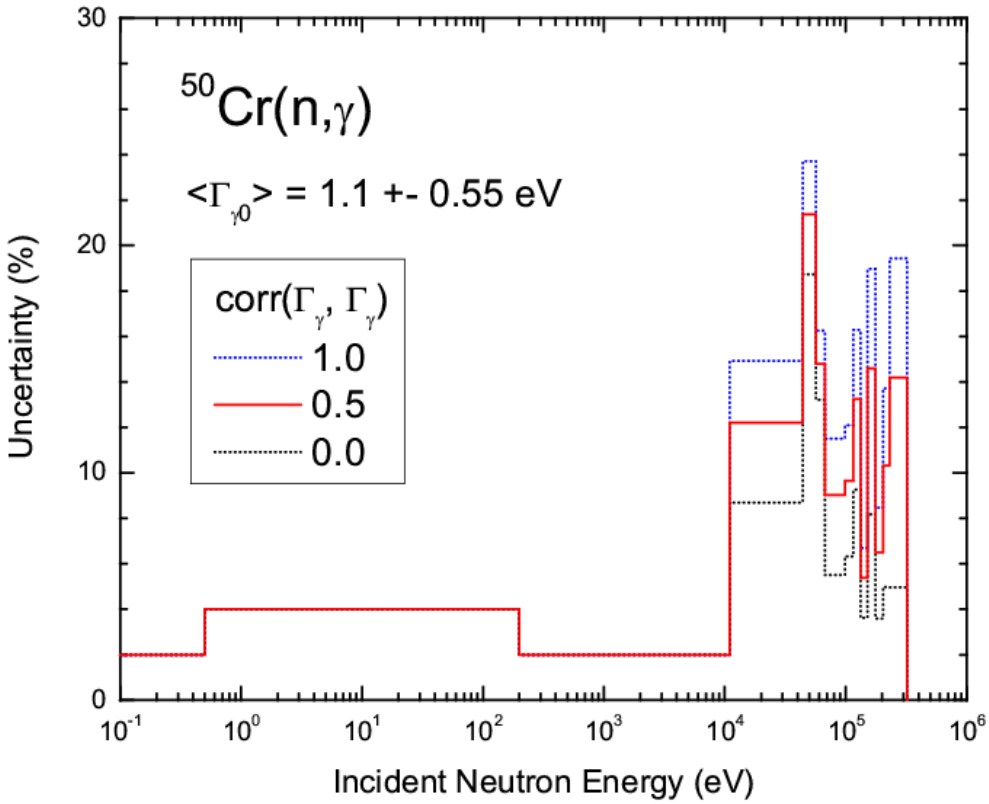

Figure 3.3: ^{50}Cr(n,γ) uncertainties for three scenarios of level-level correlation between radiative widths, corr($\Gamma_\gamma, \Gamma_\gamma$) = 1.0, 0.5 and 0.0. Above 297 keV the uncertainties of the average radiative widths were adopted, see Table 3.1.

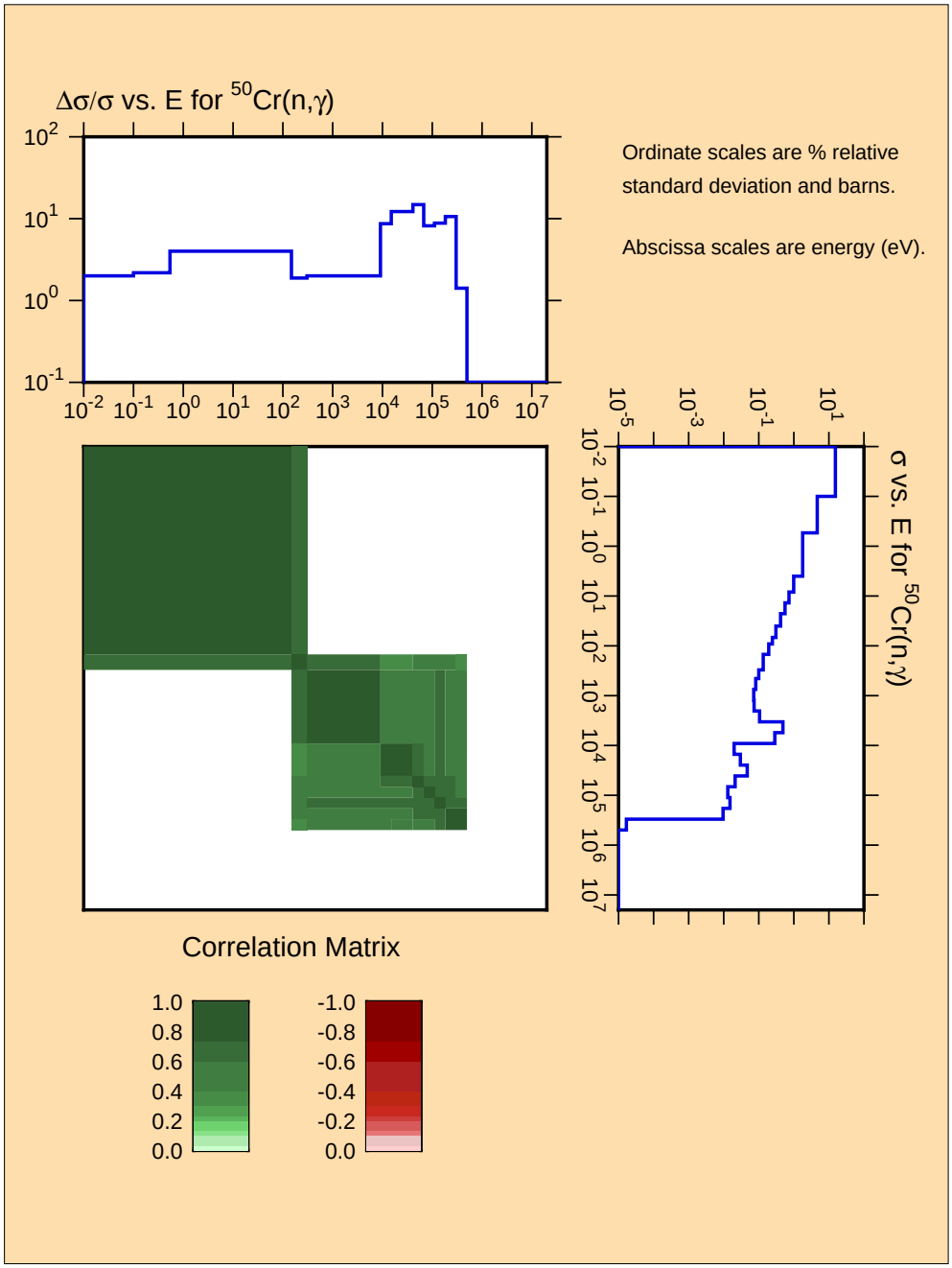

Figure 3.4: ^{50}Cr(n,γ) covariances in the thermal and resonance region for corr = 0.5, the level-level and bin-bin correlation coefficients adopted uniformly in the entire energy range. Shown are relative uncertainties in % (top), average cross sections in barns (right) and correlation matrix (bottom).

3.2.2 Elastic

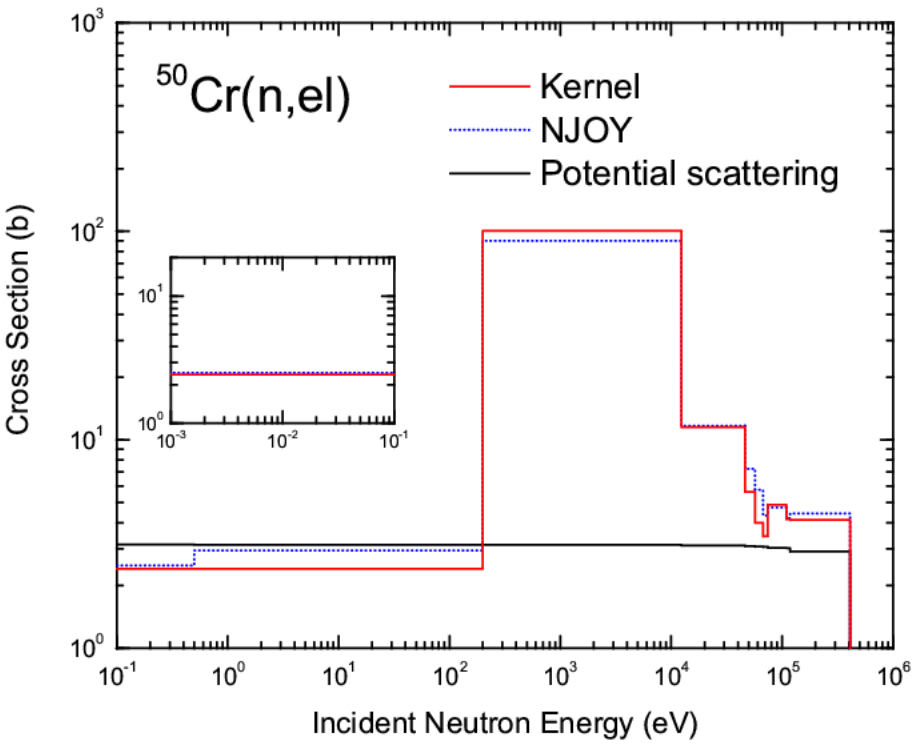

Figure 3.5: ^{50}Cr(n,el) average cross sections in the resonance region using resonance parameters from Atlas. Compared are approximate values obtained by kernel formalism with correct values obtained by NJOY. Shown in the insert is the thermal region. Potential scattering cross sections are shown explicitly, indicating strong role of potential scattering at high energies.

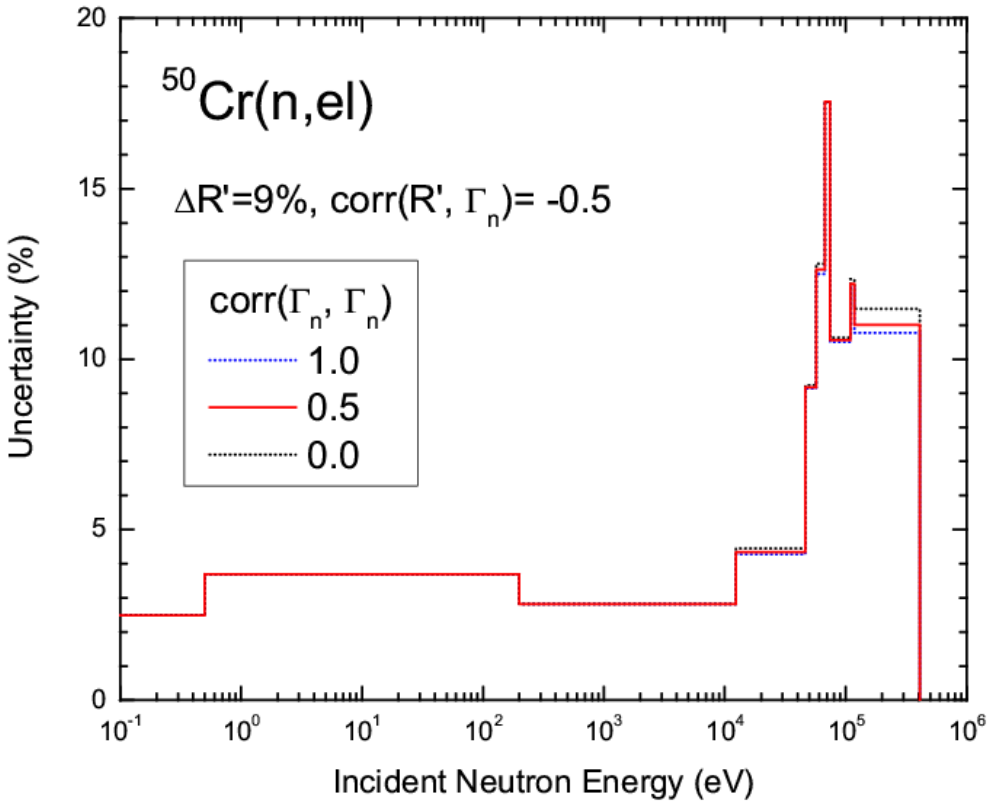

Figure 3.6: ^{50}Cr(n,el) uncertainties for three scenarios of level-level correlation between neutron widths, corr(Γ_n, Γ_n) = 1.0, 0.5 and 0.0. Assumed was scattering radius uncertainty $\Delta R'$ = 9% and default value of the correlation coefficient corr(R', Γ_n) = -0.5.

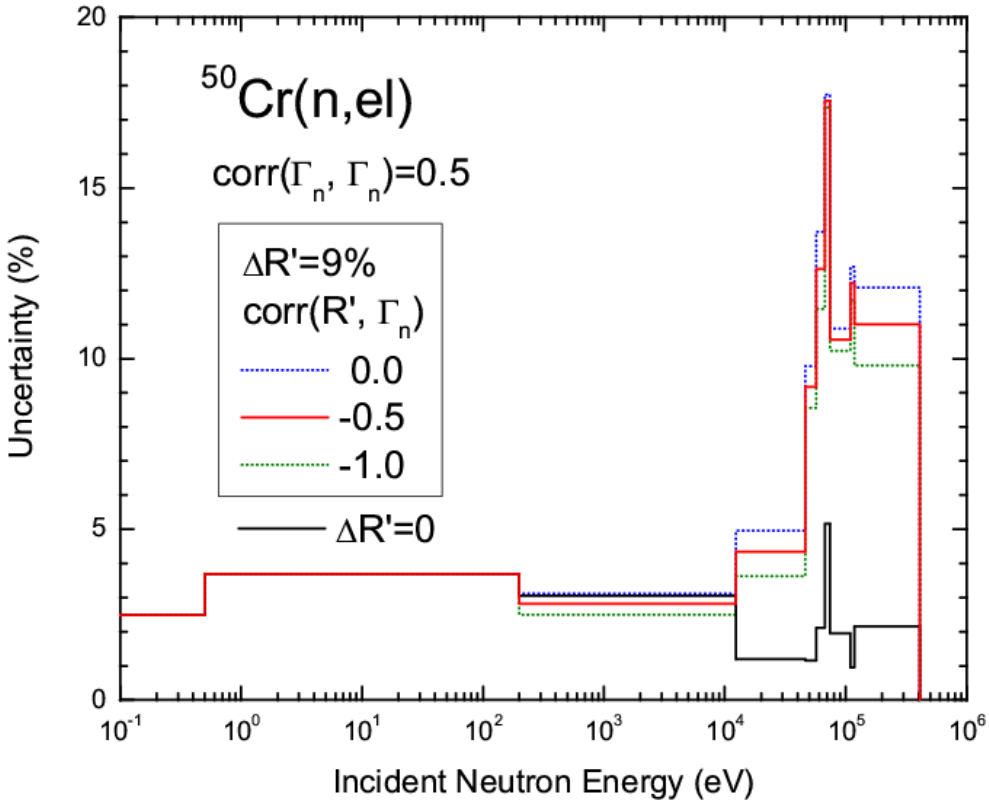

Figure 3.7: ^{50}Cr(n,el) uncertainties for three scenarios of corr(R', Γ_n) = 0.0, -0.5 and -1.0 assuming $\Delta R' = 9\%$. Shown for comparison are uncertainties assuming perfectly known scattering radius, $\Delta R' = 0$, illustrating dominant impact of $\Delta R'$ on elastic scattering cross section uncertainties at high energies.

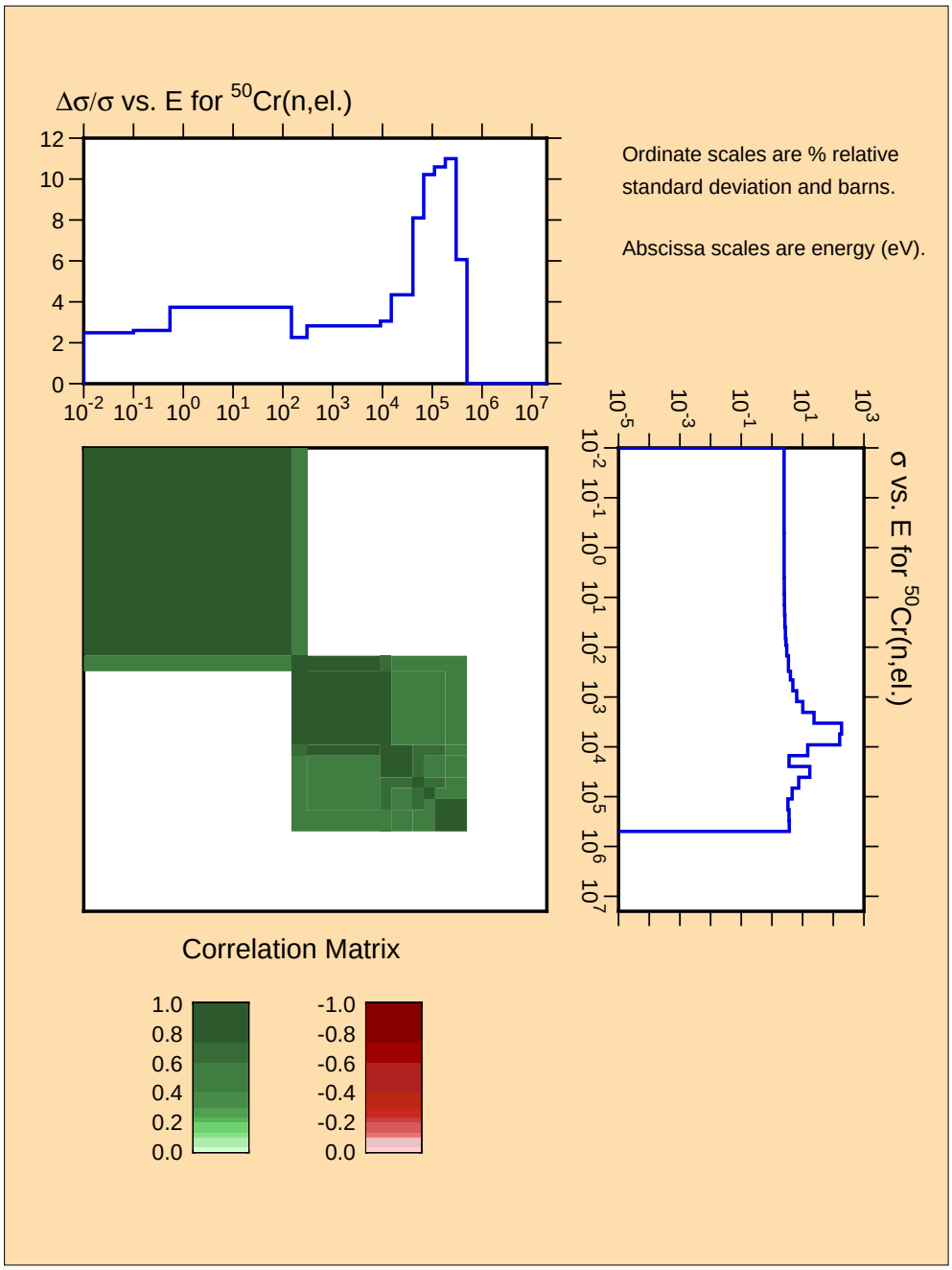

Figure 3.8: ^{50}Cr(n,el) covariances in the thermal and resonance region for the uniformly adopted value of level-level and bin-bin correlation coefficients, corr = 0.5.

3.3 ^{53}Cr evaluation

Evaluation is performed in several consecutive steps. We start with inspecting capture and elastic scattering cross sections in ENDF/B-VII.0 library. Then, we identify the proper energy binning for average cross sections, compute uncertainties for the average cross sections in these energy bins, and finally combine the bins into covariance matrix. Details can be seen on subsequent plots.

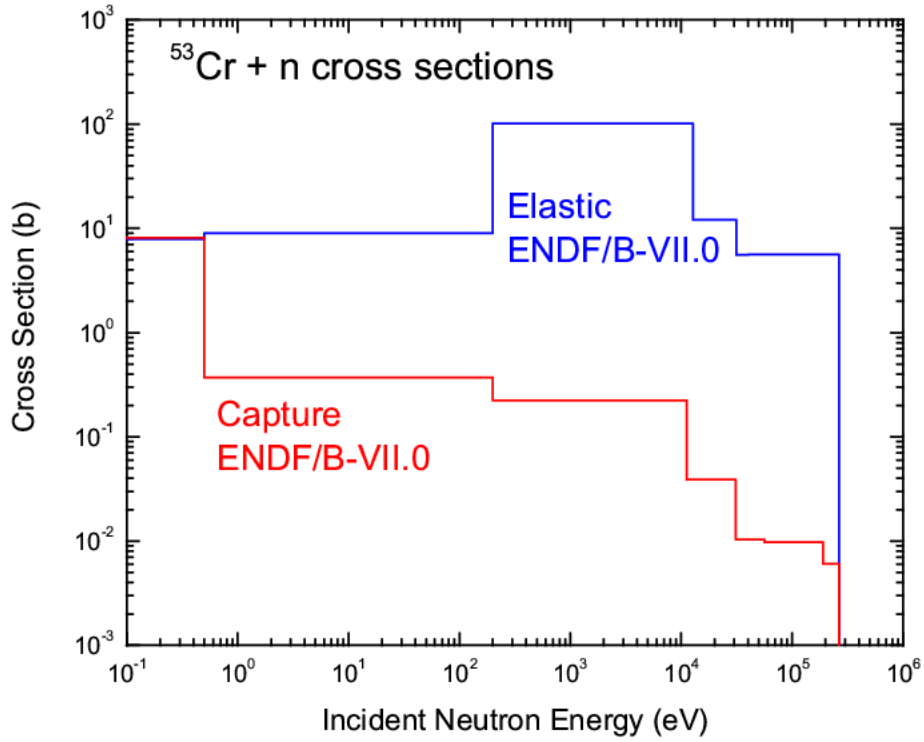

Figure 3.9: ^{53}Cr(n,γ) and (n,el) average cross sections in the thermal and resonance region using resonance parameters from ENDF/B-VII.0 processed by NJOY.

3.3.1 Capture

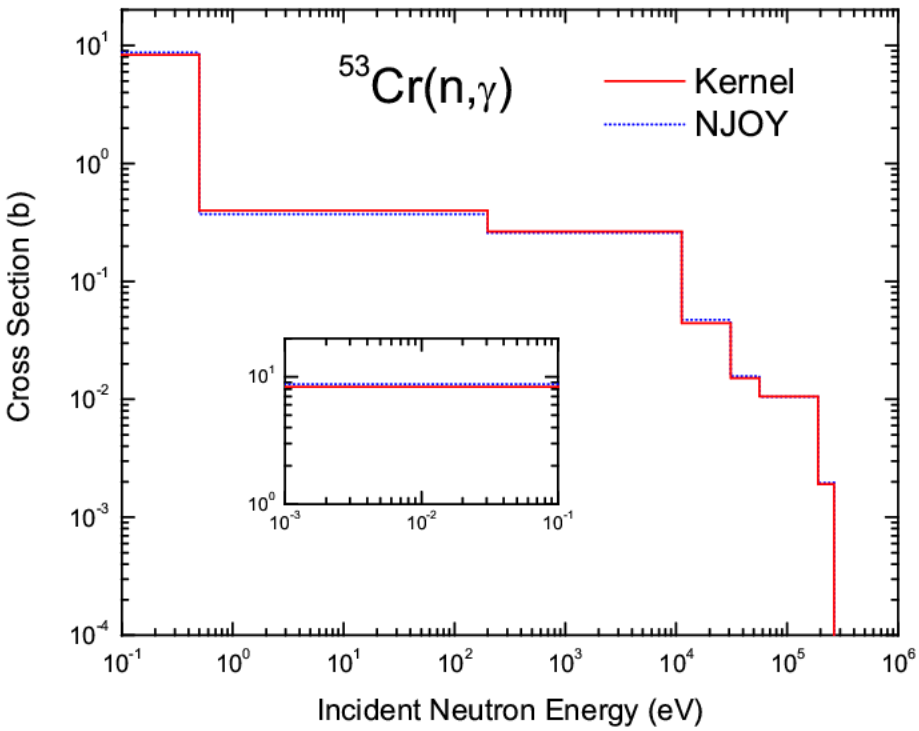

Figure 3.10: ^{53}Cr(n,γ) average cross sections using resonance parameters from Atlas. Compared are approximate values obtained by kernel formalism with correct values obtained by NJOY, demonstrating an excellent agreement. Shown in the insert is the thermal region.

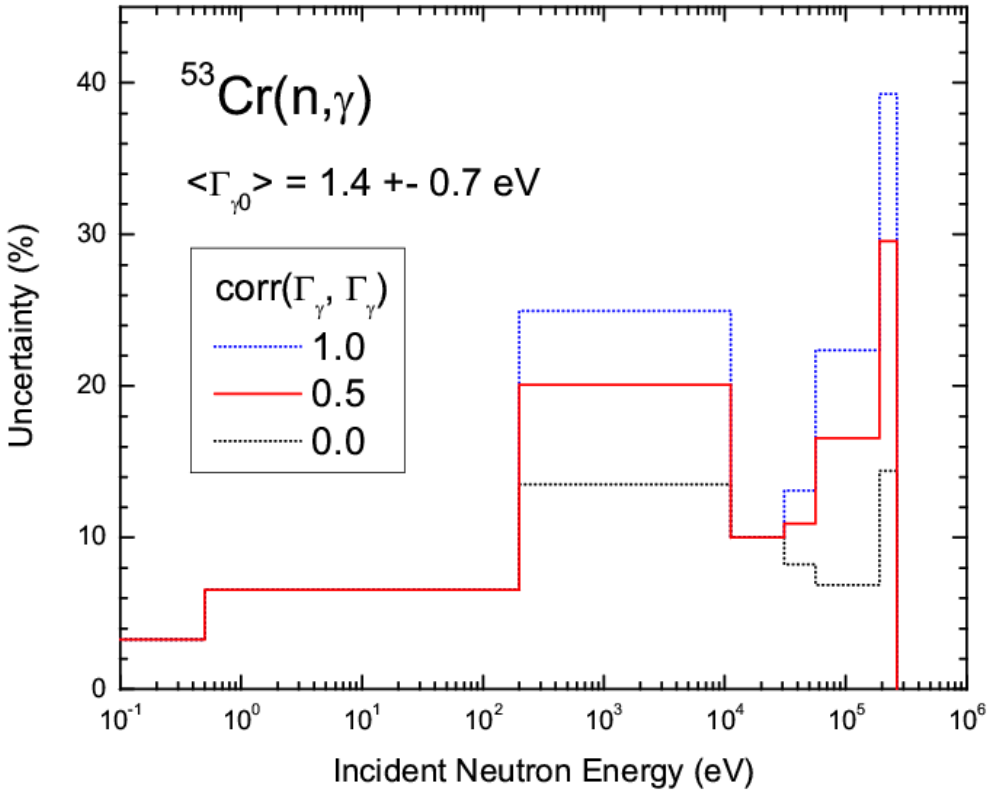

Figure 3.11: ^{53}Cr(n,γ) uncertainties for three scenarios of level-level correlation between radiative widths, corr($\Gamma_\gamma, \Gamma_\gamma$) = 1.0, 0.5 and 0.0. Above 200 keV the uncertainties of the average radiative widths were adopted, see Table 3.1.

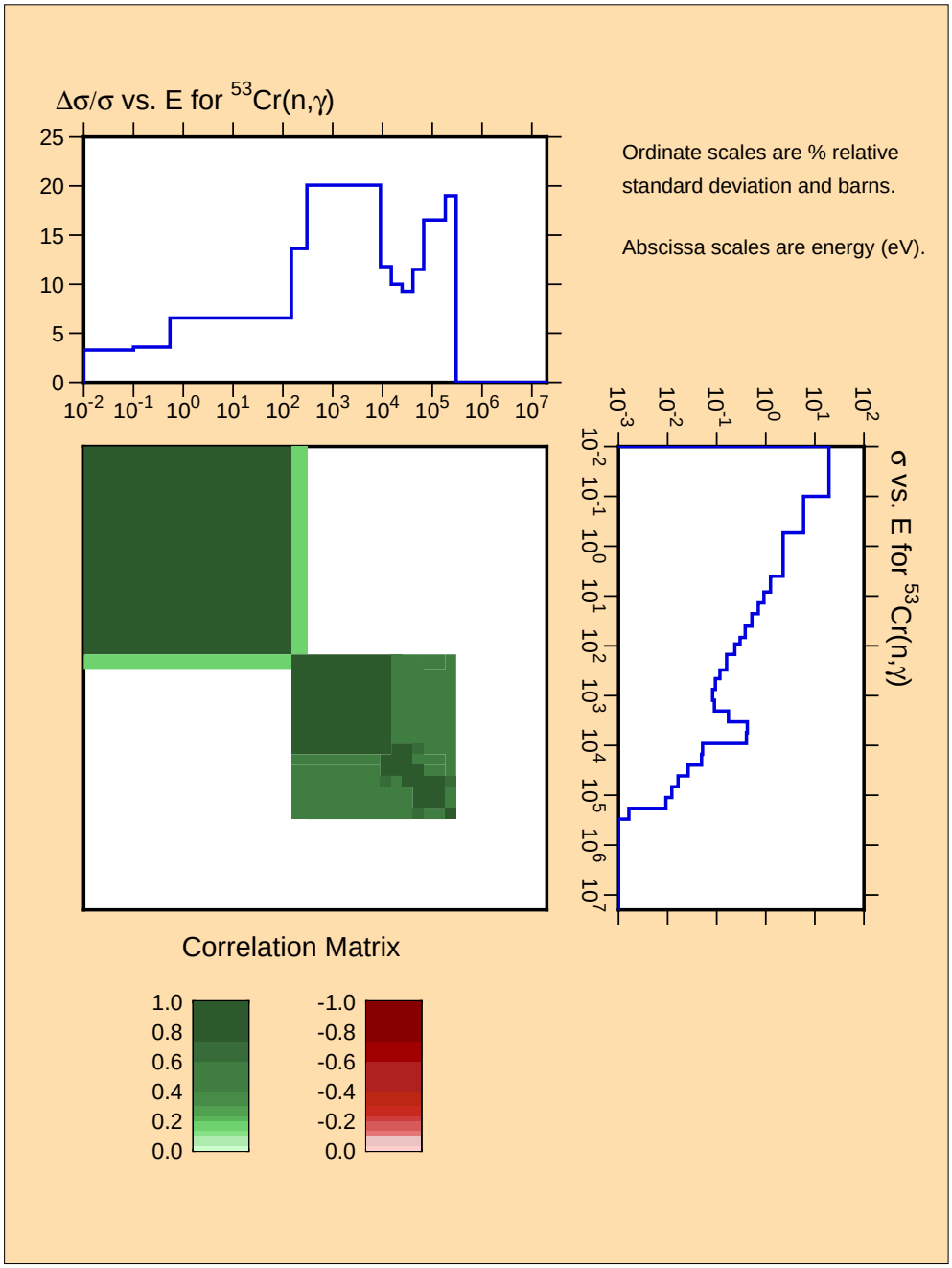

Figure 3.12: ^{53}Cr(n,γ) covariances in the thermal and resonance region for corr = 0.5, the level-level and bin-bin correlation coefficients adopted uniformly in the entire energy range. Shown are relative uncertainties in % (top), average cross sections in barns (right) and correlation matrix (bottom).

3.3.2 Elastic

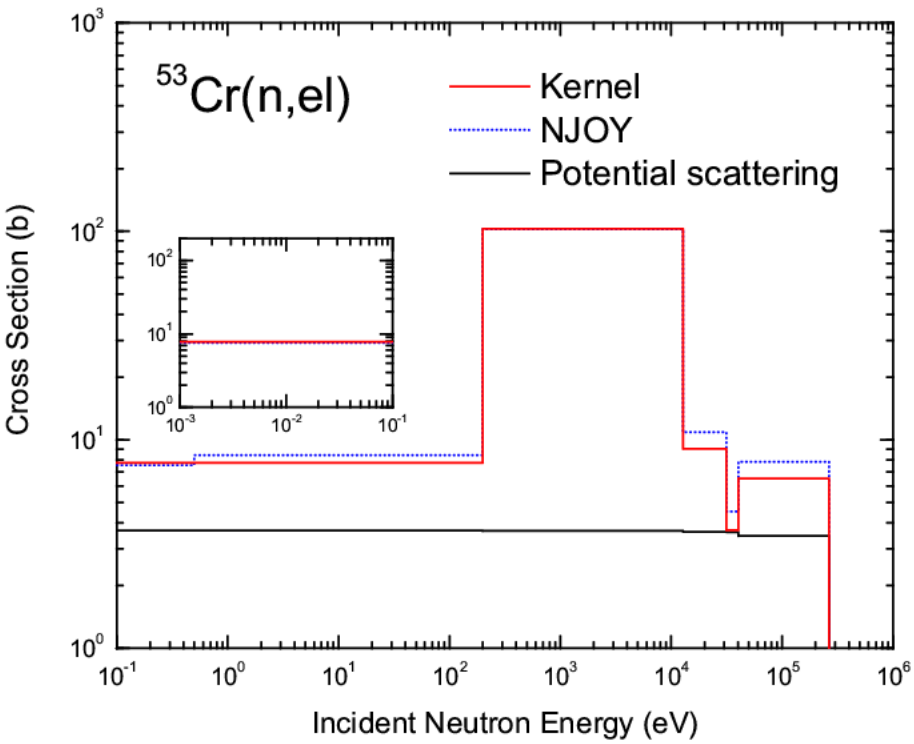

Figure 3.13: ^{53}Cr(n,el) average cross sections in the resonance region using resonance parameters from Atlas. Compared are approximate values obtained by kernel formalism with correct values obtained by NJOY. Shown in the insert is the thermal region. Potential scattering cross sections are shown explicitly, indicating strong role of potential scattering at high energies.

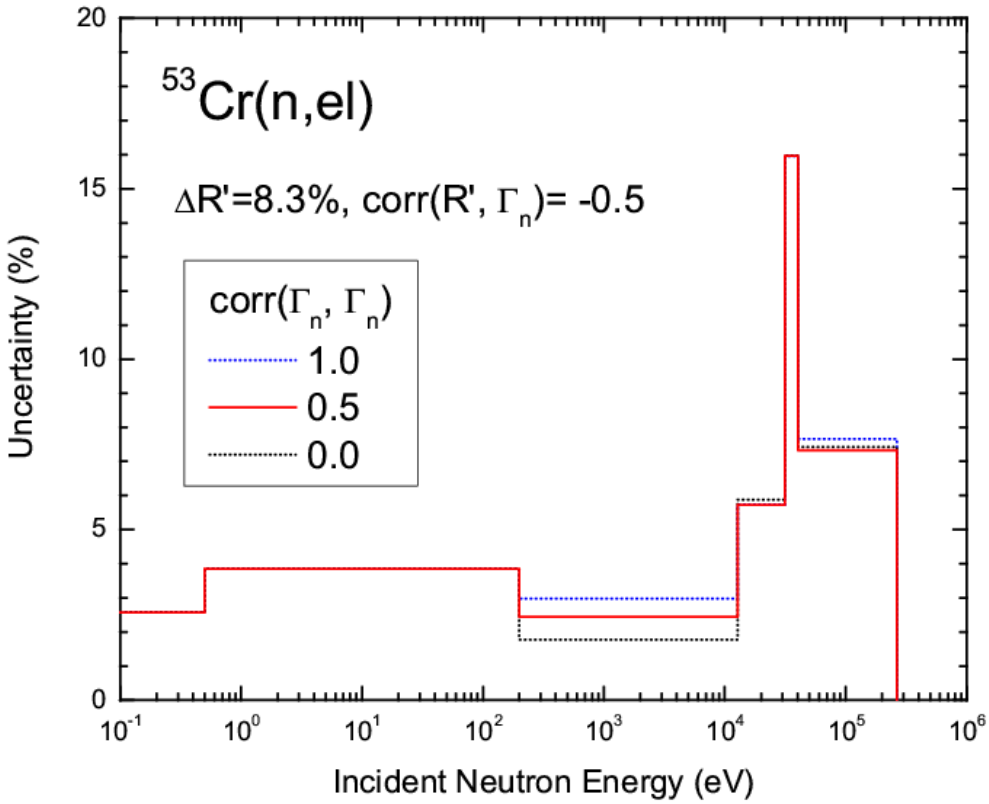

Figure 3.14: ^{53}Cr(n,el) uncertainties for three scenarios of level-level correlation between neutron widths, corr(Γ_n, Γ_n) = 1.0, 0.5 and 0.0. Assumed was scattering radius uncertainty $\Delta R'$ = 8.3% and default value of the correlation coefficient corr(R', Γ_n) = -0.5.

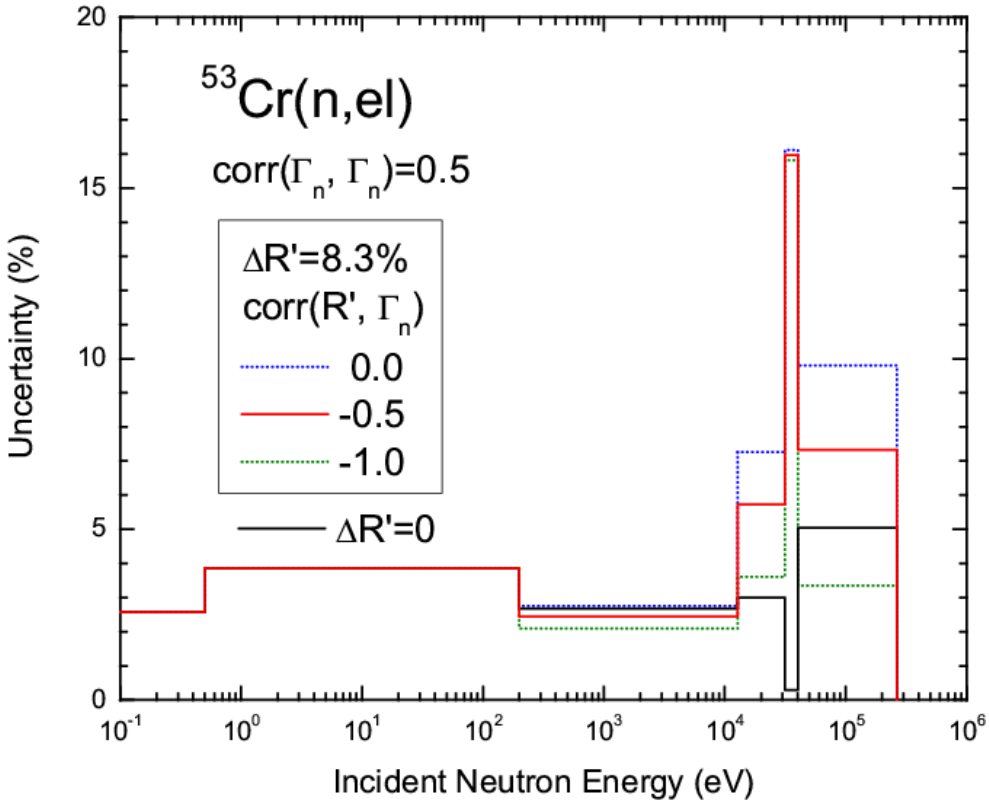

Figure 3.15: ^{53}Cr(n,el) uncertainties for three scenarios of corr(R', Γ_n) = 0.0, -0.5 and -1.0 assuming $\Delta R'$ = 8.3%. Shown for comparison are uncertainties assuming perfectly known scattering radius, $\Delta R'$ = 0, illustrating strong impact of $\Delta R'$ on elastic scattering cross section uncertainties at high energies.

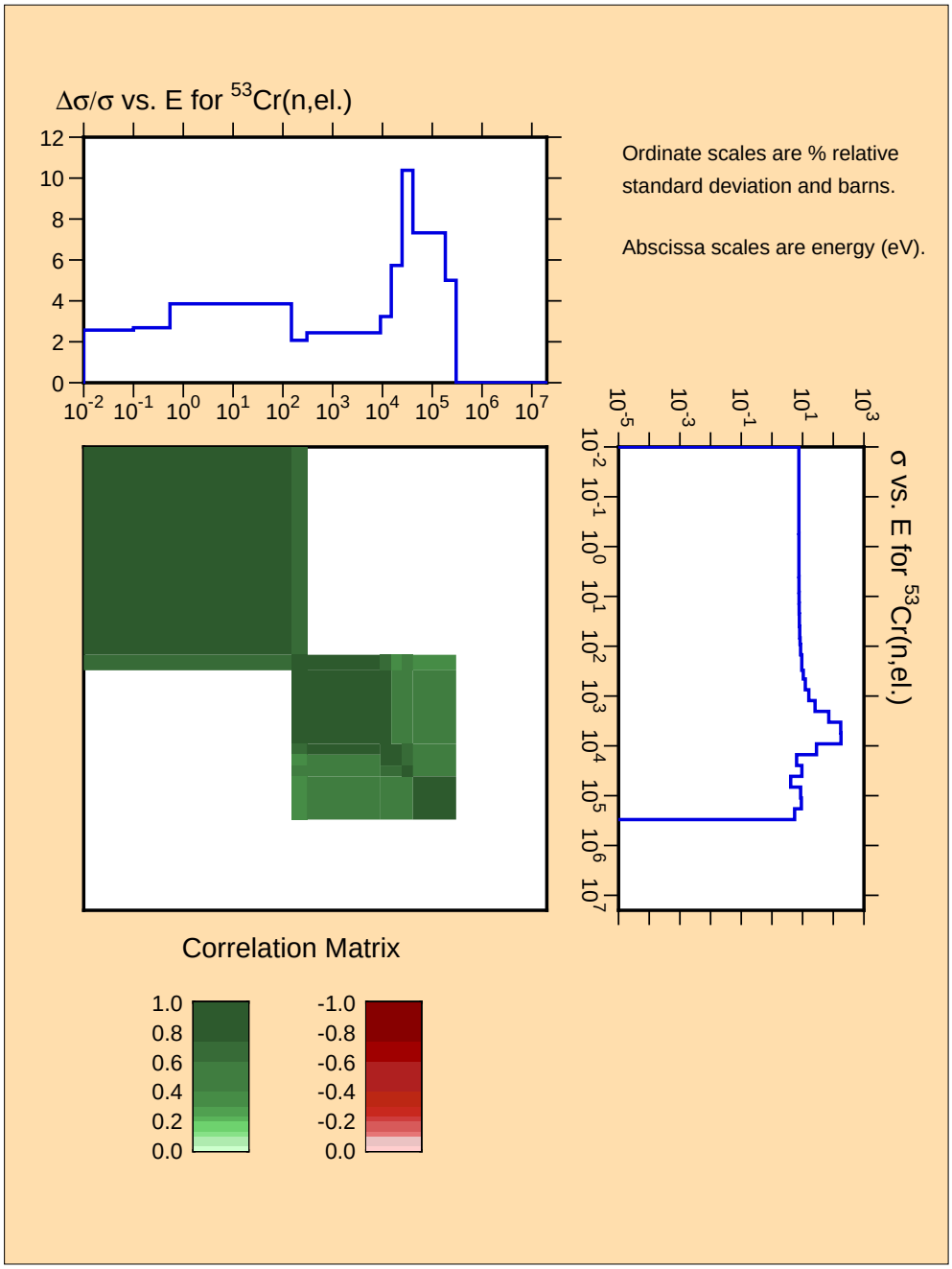

Figure 3.16: ^{53}Cr(n,el) covariances in the thermal and resonance region for the uniformly adopted value of level-level and bin-bin correlation coefficients, corr = 0.5.

3.4 ^{54}Fe evaluation

Evaluation is performed in several consecutive steps. We start with inspecting capture and elastic scattering cross sections in ENDF/B-VII.0 library. Then, we identify the proper energy binning for average cross sections, compute uncertainties for the average cross sections in these energy bins, and finally combine the bins into covariance matrix. Details can be seen on subsequent plots.

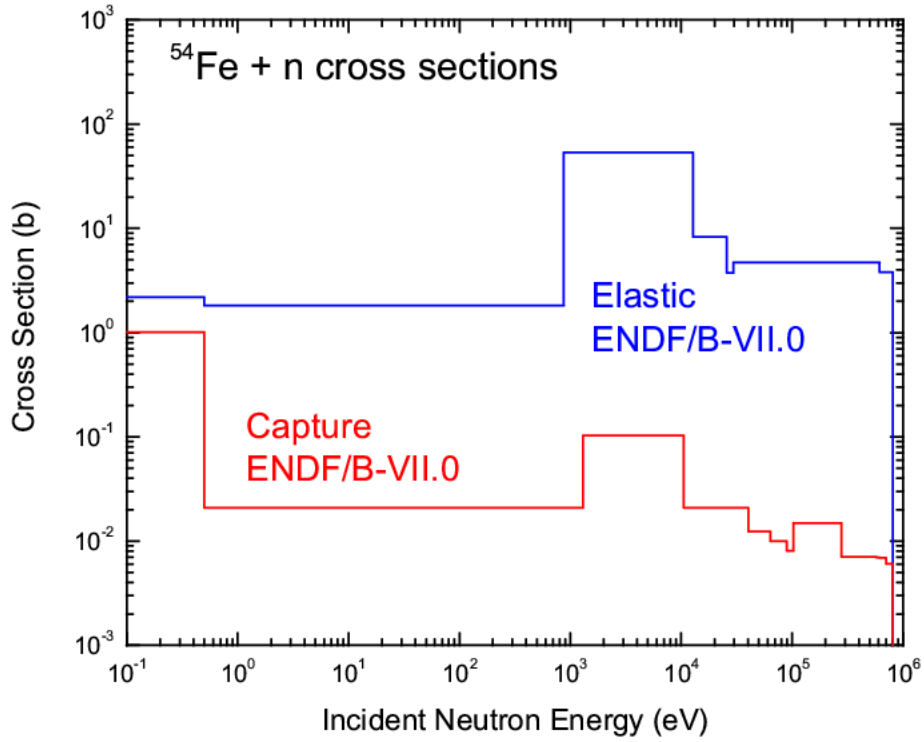

Figure 3.17: ^{54}Fe(n,γ) and (n,el) average cross sections in the thermal and resonance region using resonance parameters from ENDF/B-VII.0 processed by NJOY.

3.4.1 Capture

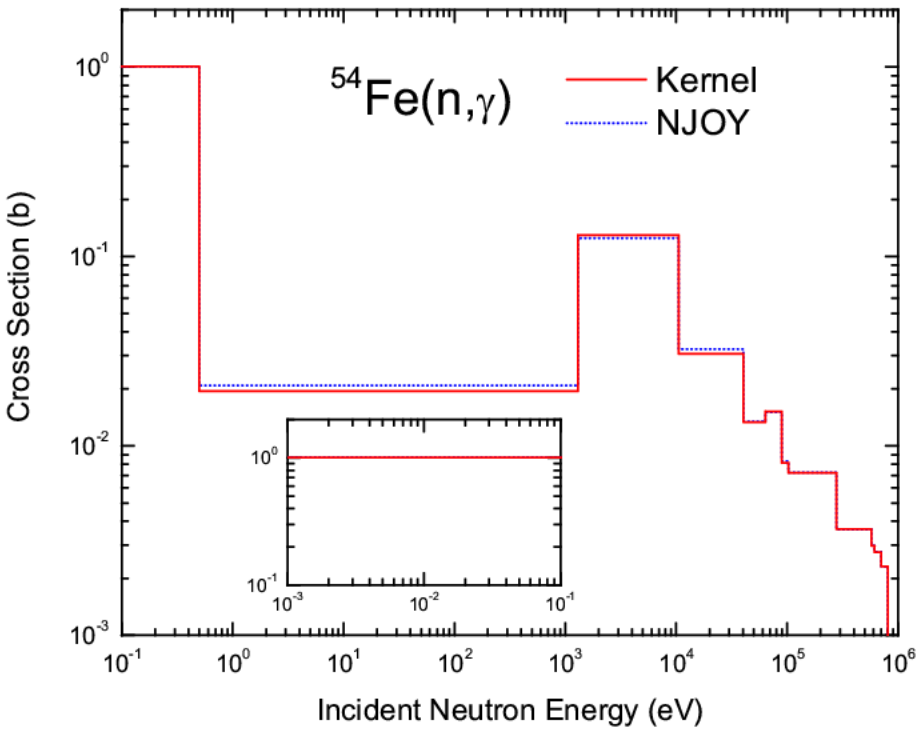

Figure 3.18: ^{54}Fe(n,γ) average cross sections using resonance parameters from Atlas. Compared are approximate values obtained by kernel formalism with correct values obtained by NJOY, demonstrating an excellent agreement. Shown in the insert is the thermal region.

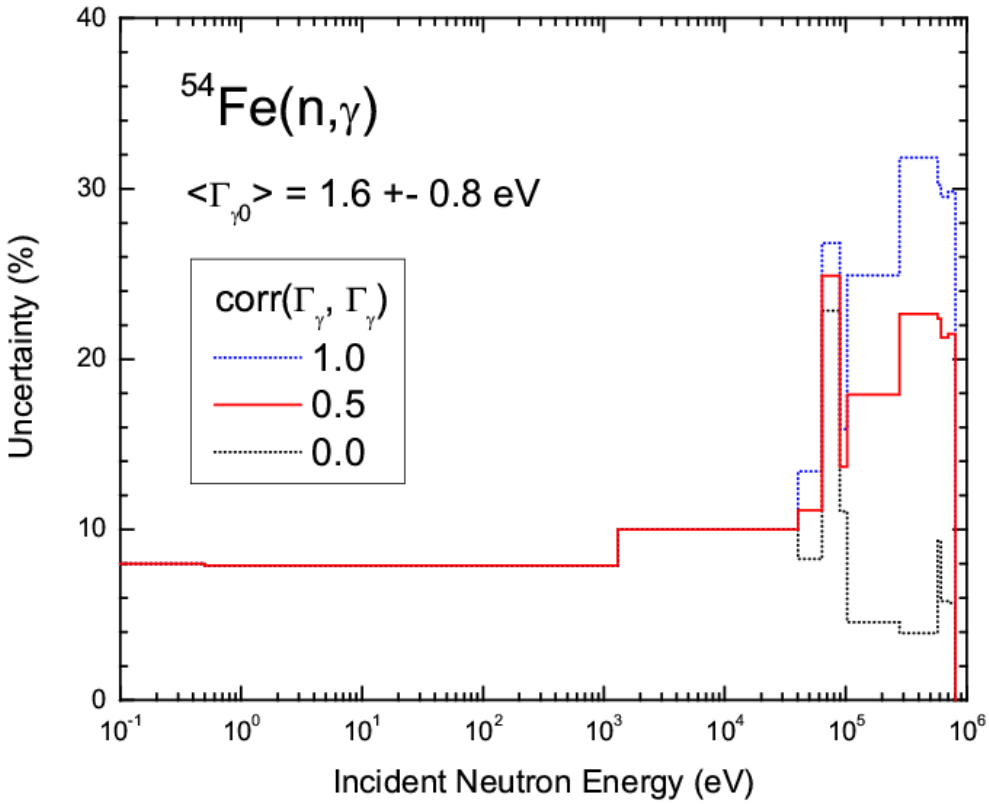

Figure 3.19: ^{54}Fe(n,γ) uncertainties for three scenarios of level-level correlation between radiative widths, corr($\Gamma_\gamma, \Gamma_\gamma$) = 1.0, 0.5 and 0.0. Above 195 keV the uncertainties of the average radiative widths were adopted, see Table 3.1.

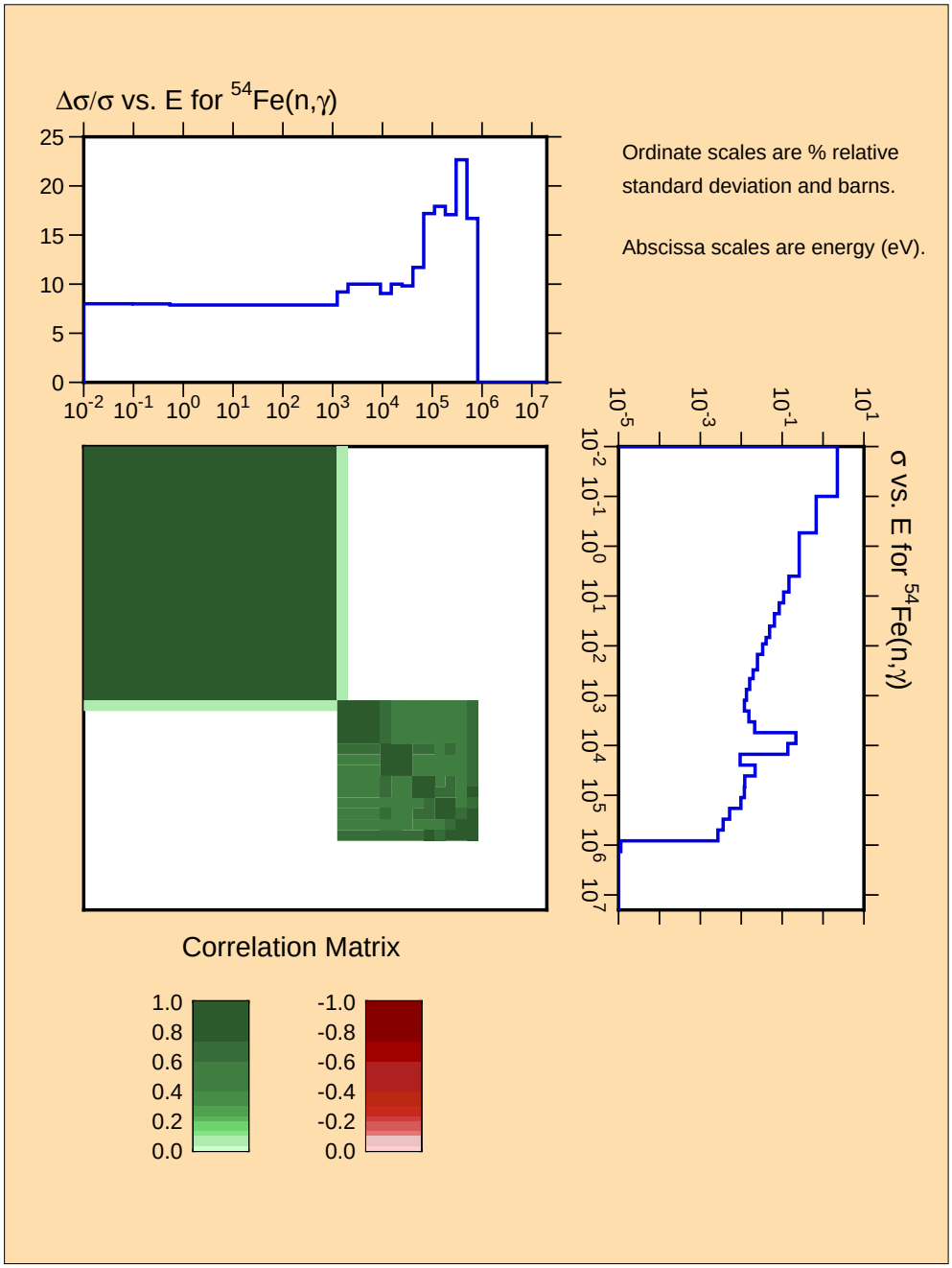

Figure 3.20: ^{54}Fe(n,γ) covariances in the thermal and resonance region for corr = 0.5, the level-level and bin-bin correlation coefficients adopted uniformly in the entire energy range. Shown are relative uncertainties in % (top), average cross sections in barns (right) and correlation matrix (bottom).

3.4.2 Elastic

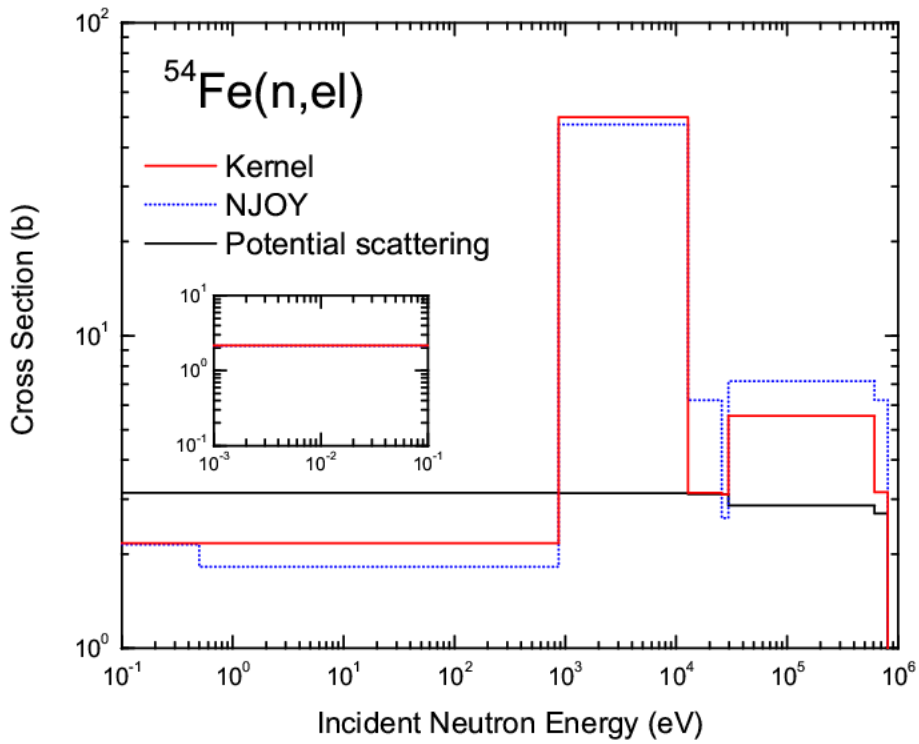

Figure 3.21: ^{54}Fe(n,el) average cross sections in the thermal and resonance region for resonance parameters from Atlas. Compared are approximate values obtained by kernel formalism with correct values obtained by NJOY. Shown in the insert is the thermal region. Potential scattering cross sections are shown explicitly, indicating strong role of potential scattering at high energies.

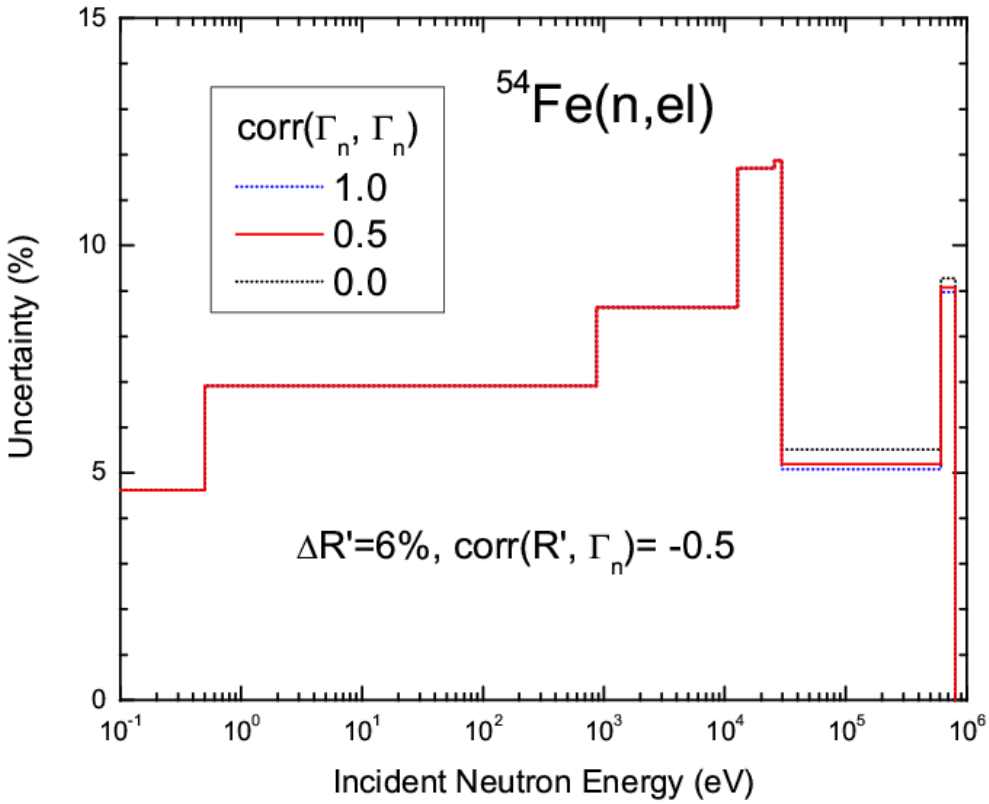

Figure 3.22: ^{54}Fe(n,el) uncertainties for three scenarios of level-level correlation between neutron widths, corr(Γ_n, Γ_n) = 1.0, 0.5 and 0.0. Assumed was scattering radius uncertainty $\Delta R' = 6\%$ and default value of the correlation coefficient corr(R', Γ_n) = -0.5.

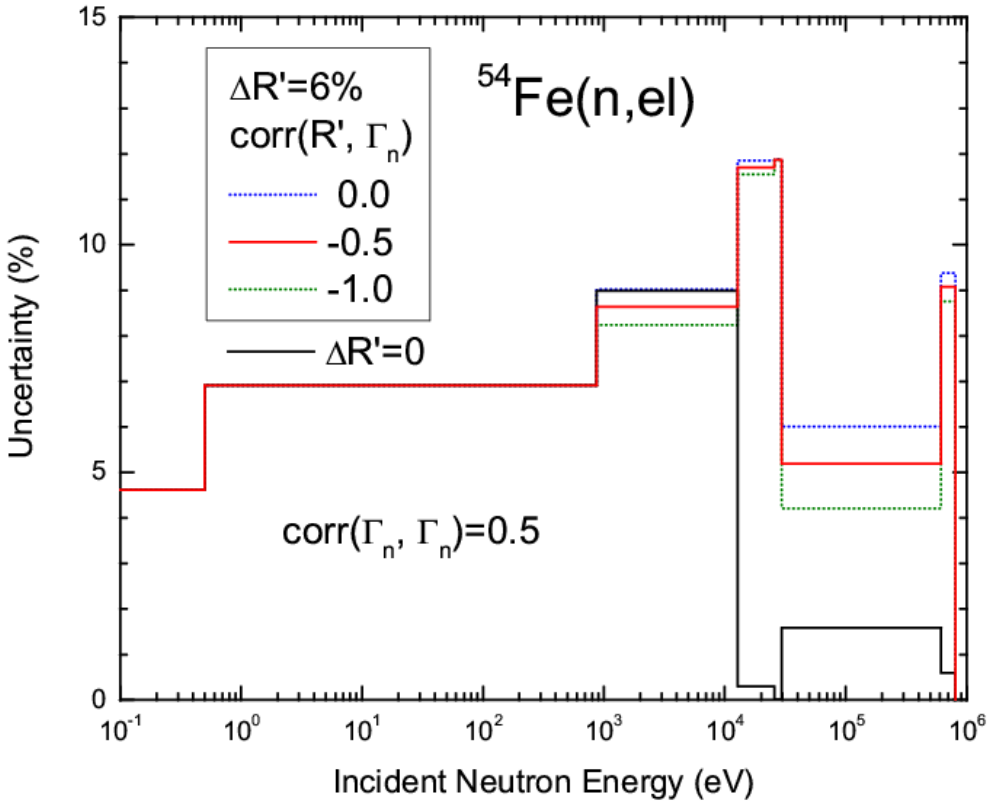

Figure 3.23: ^{54}Fe(n,el) uncertainties for three scenarios of corr(R', Γ_n) = 0.0, -0.5 and -1.0 assuming $\Delta R' = 6\%$. Shown for comparison are uncertainties assuming perfectly known scattering radius, $\Delta R' = 0$, illustrating dominant impact of $\Delta R'$ on elastic scattering cross section uncertainties at high energies.

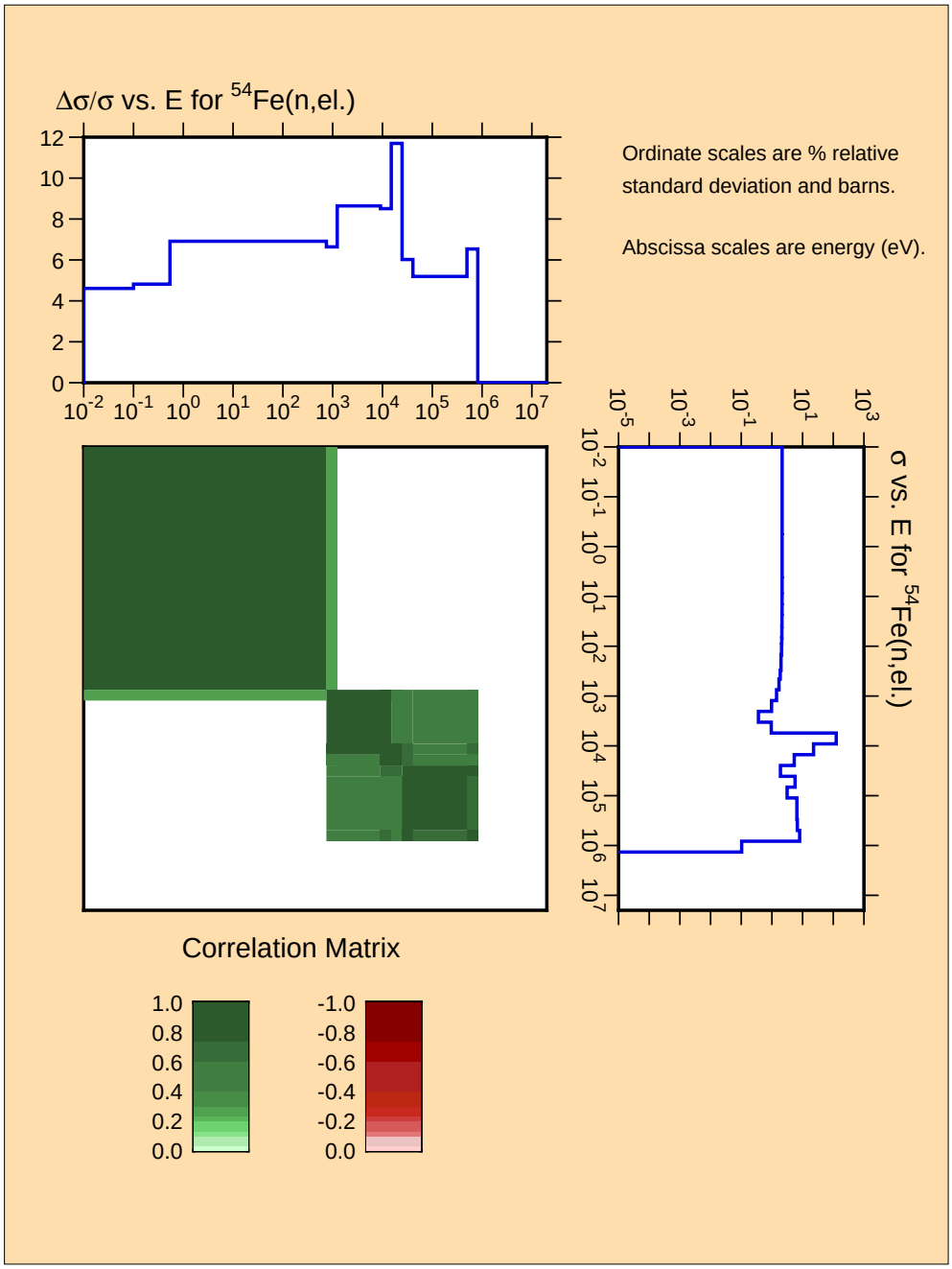

Figure 3.24: ^{54}Fe(n,el) covariances in the thermal and resonance region for the uniformly adopted value of level-level and bin-bin correlation coefficients, corr = 0.5.

3.5 ^{57}Fe evaluation

Evaluation is performed in several consecutive steps. We start with inspecting capture and elastic scattering cross sections in ENDF/B-VII.0 library. Then, we identify the proper energy binning for average cross sections, compute uncertainties for the average cross sections in these energy bins, and finally combine the bins into covariance matrix. Details can be seen on subsequent plots.

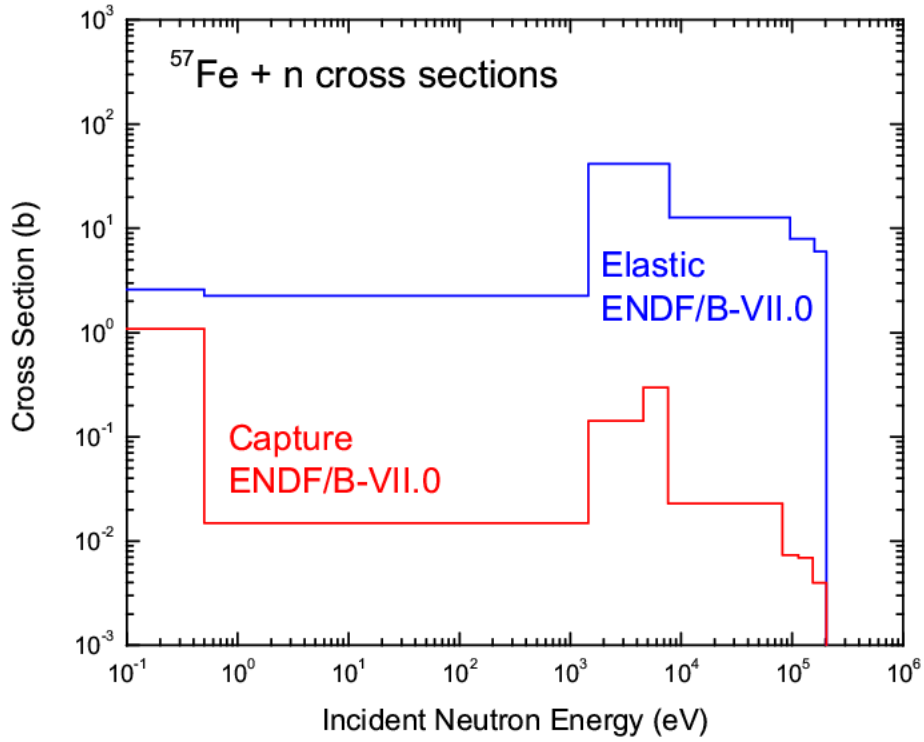

Figure 3.25: ^{57}Fe(n,γ) and (n,el) average cross sections in the thermal and resonance region using resonance parameters from ENDF/B-VII.0 processed by NJOY.

3.5.1 Capture

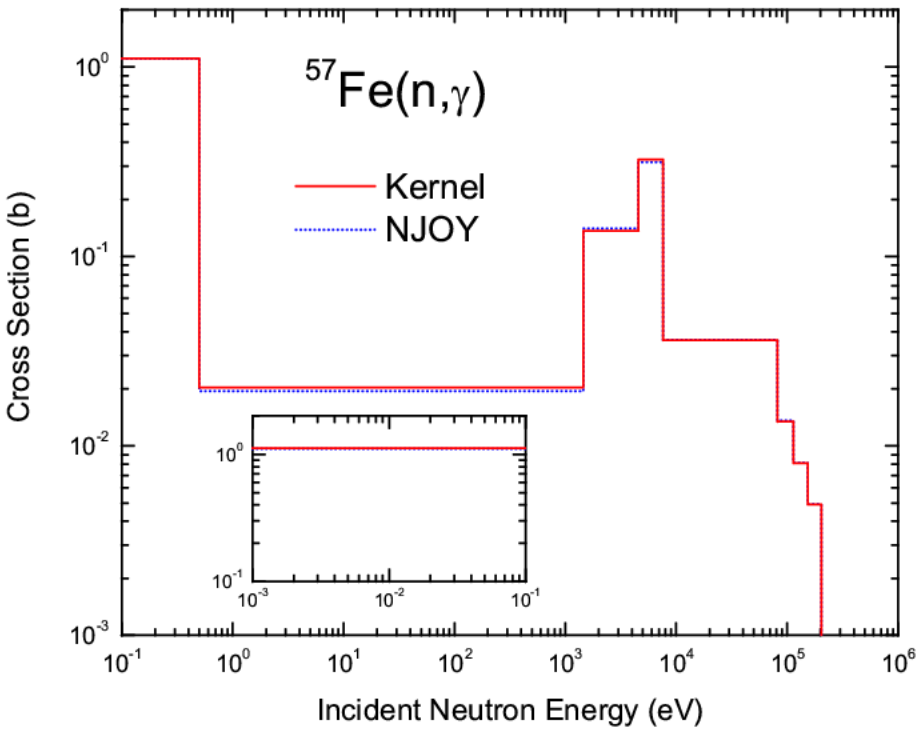

Figure 3.26: ^{57}Fe(n,γ) average cross sections using resonance parameters from Atlas. Compared are approximate values obtained by kernel formalism with correct values obtained by NJOY, demonstrating an excellent agreement. Shown in the insert is the thermal region.

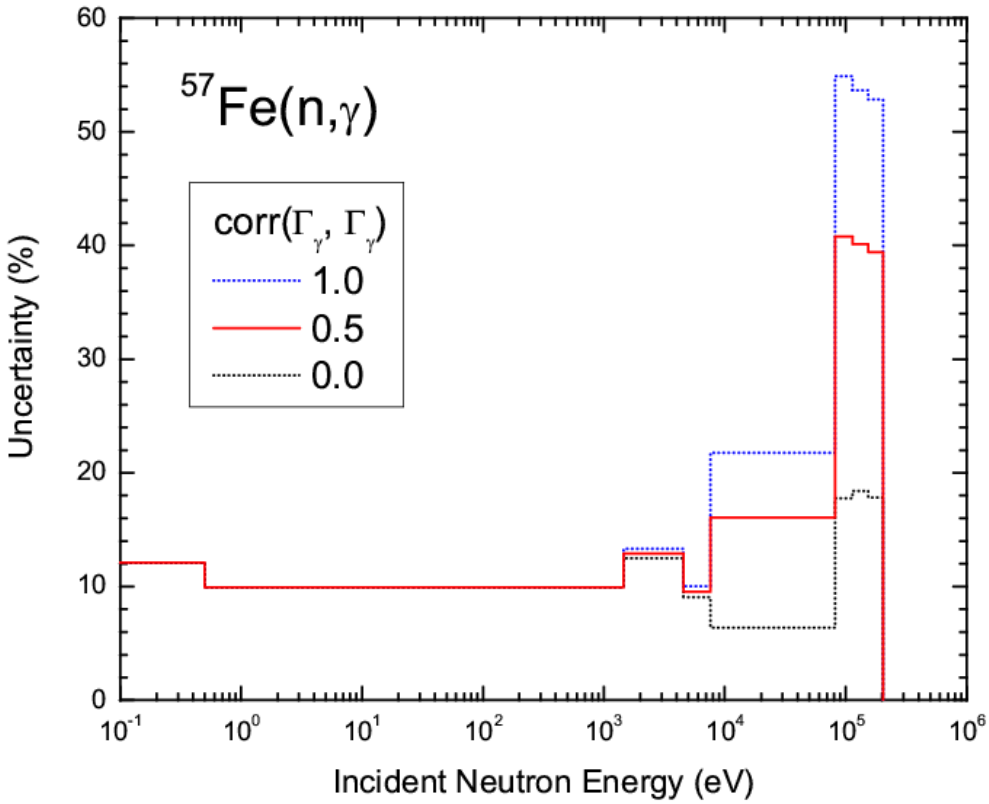

Figure 3.27: ^{57}Fe(n,γ) uncertainties for three scenarios of level-level correlation between radiative widths, corr($\Gamma_\gamma, \Gamma_\gamma$) = 1.0, 0.5 and 0.0. Above 190 keV the uncertainties of the average radiative widths were adopted, see Table 3.1.

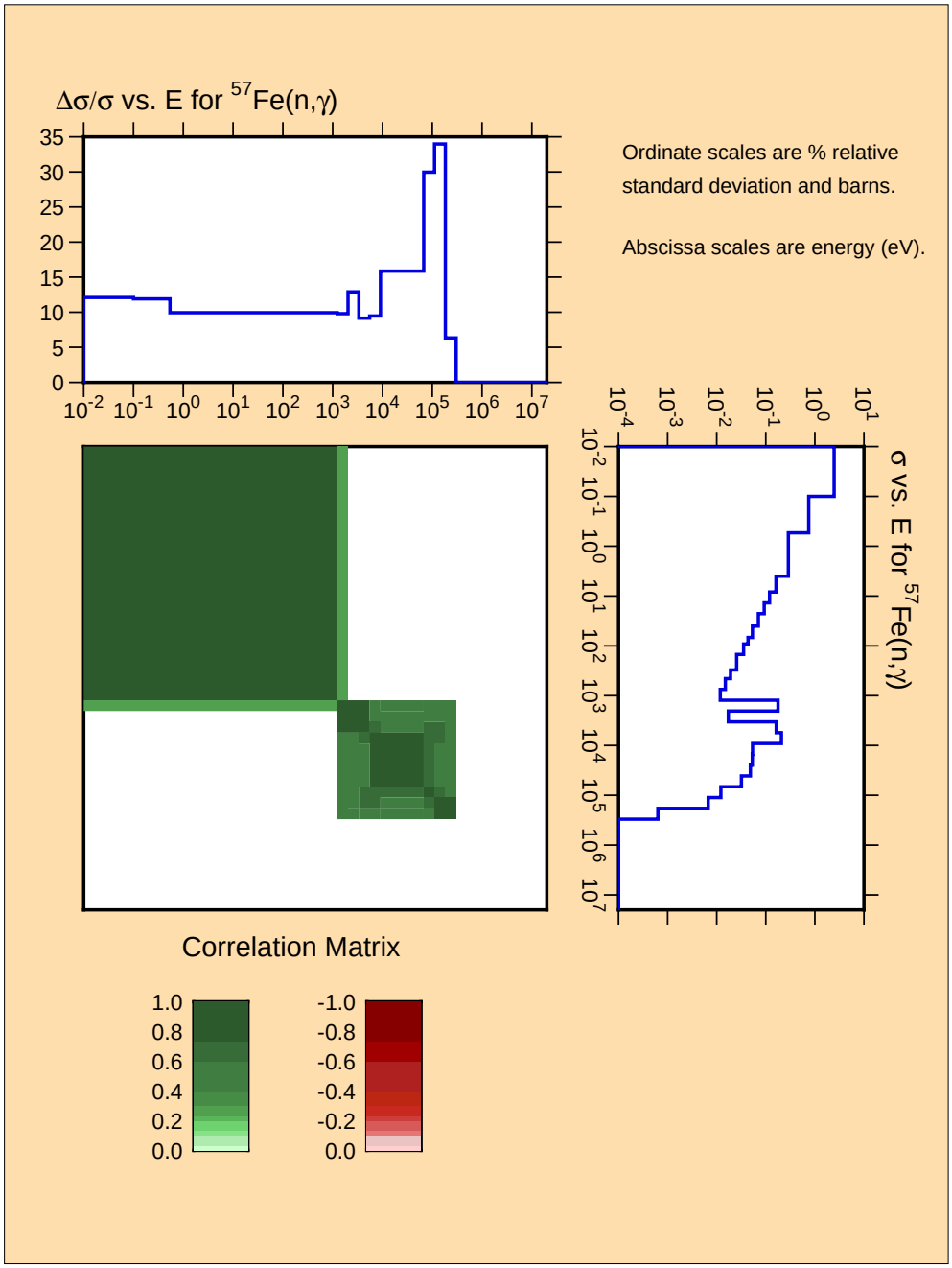

Figure 3.28: ^{57}Fe(n,γ) covariances in the thermal and resonance region for corr = 0.5, the level-level and bin-bin correlation coefficients adopted uniformly in the entire energy range. Shown are relative uncertainties in % (top), average cross sections in barns (right) and correlation matrix (bottom).

3.5.2 Elastic

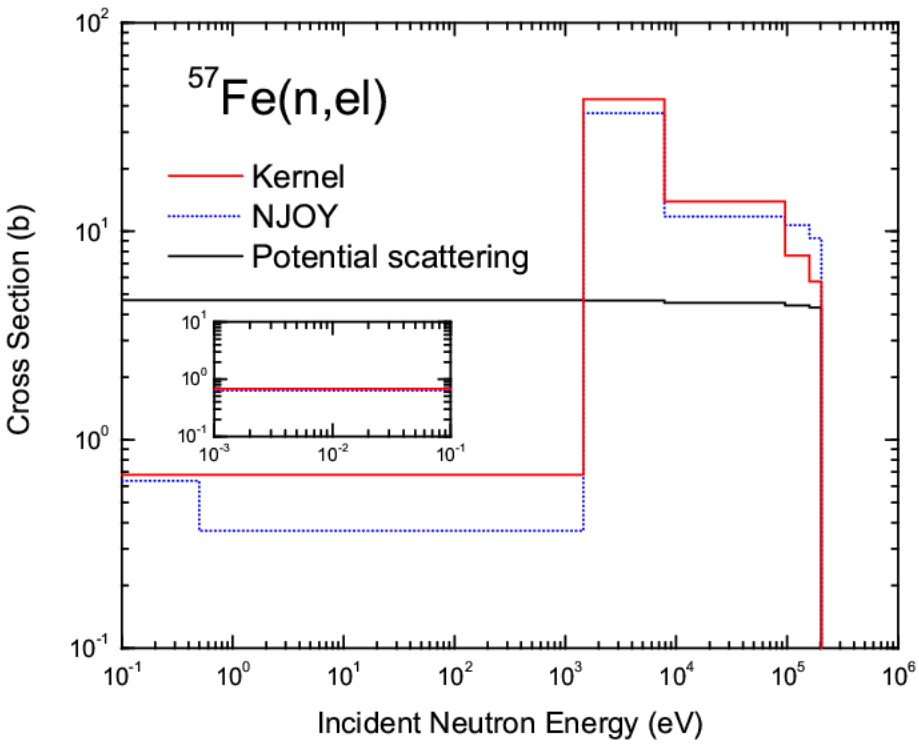

Figure 3.29: ^{57}Fe(n,el) average cross sections in the resonance region using resonance parameters from Atlas. Compared are approximate values obtained by kernel formalism with correct values obtained by NJOY. Shown in the insert is the thermal region. Potential scattering cross sections are shown explicitly, indicating strong role of potential scattering at high energies.

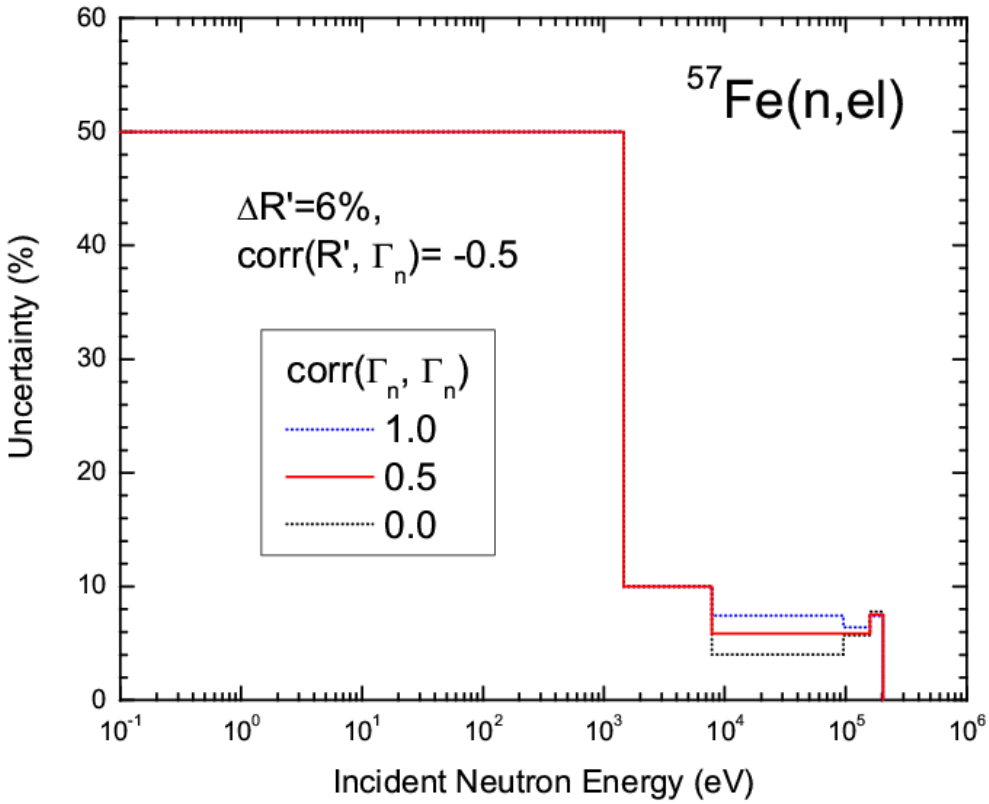

Figure 3.30: ^{57}Fe(n,el) uncertainties for three scenarios of level-level correlation between neutron widths, corr(Γ_n, Γ_n) = 1.0, 0.5 and 0.0. Assumed was scattering radius uncertainty $\Delta R'$ = 6% and default value of the correlation coefficient corr(R', Γ_n) = -0.5.

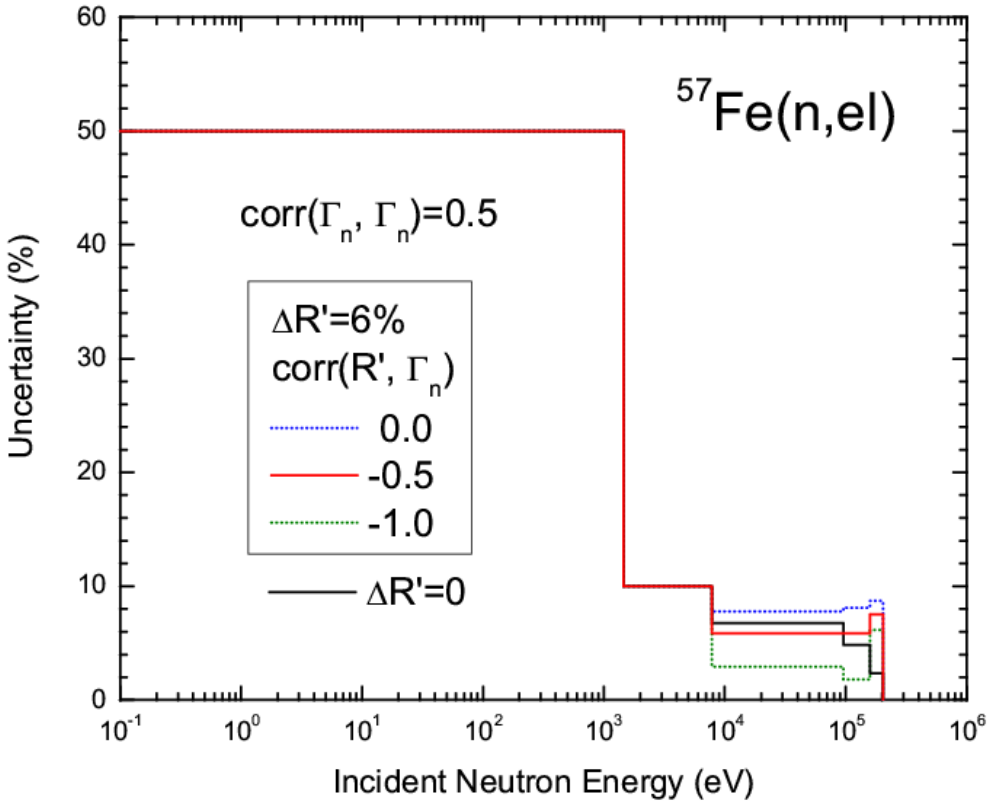

Figure 3.31: ^{57}Fe(n,el) uncertainties for three scenarios of corr(R', Γ_n) = 0.0, -0.5 and -1.0 assuming $\Delta R' = 6\%$. Shown for comparison are uncertainties assuming perfectly known scattering radius, $\Delta R' = 0$, illustrating dominant impact of $\Delta R'$ on elastic scattering cross section uncertainties at high energies.

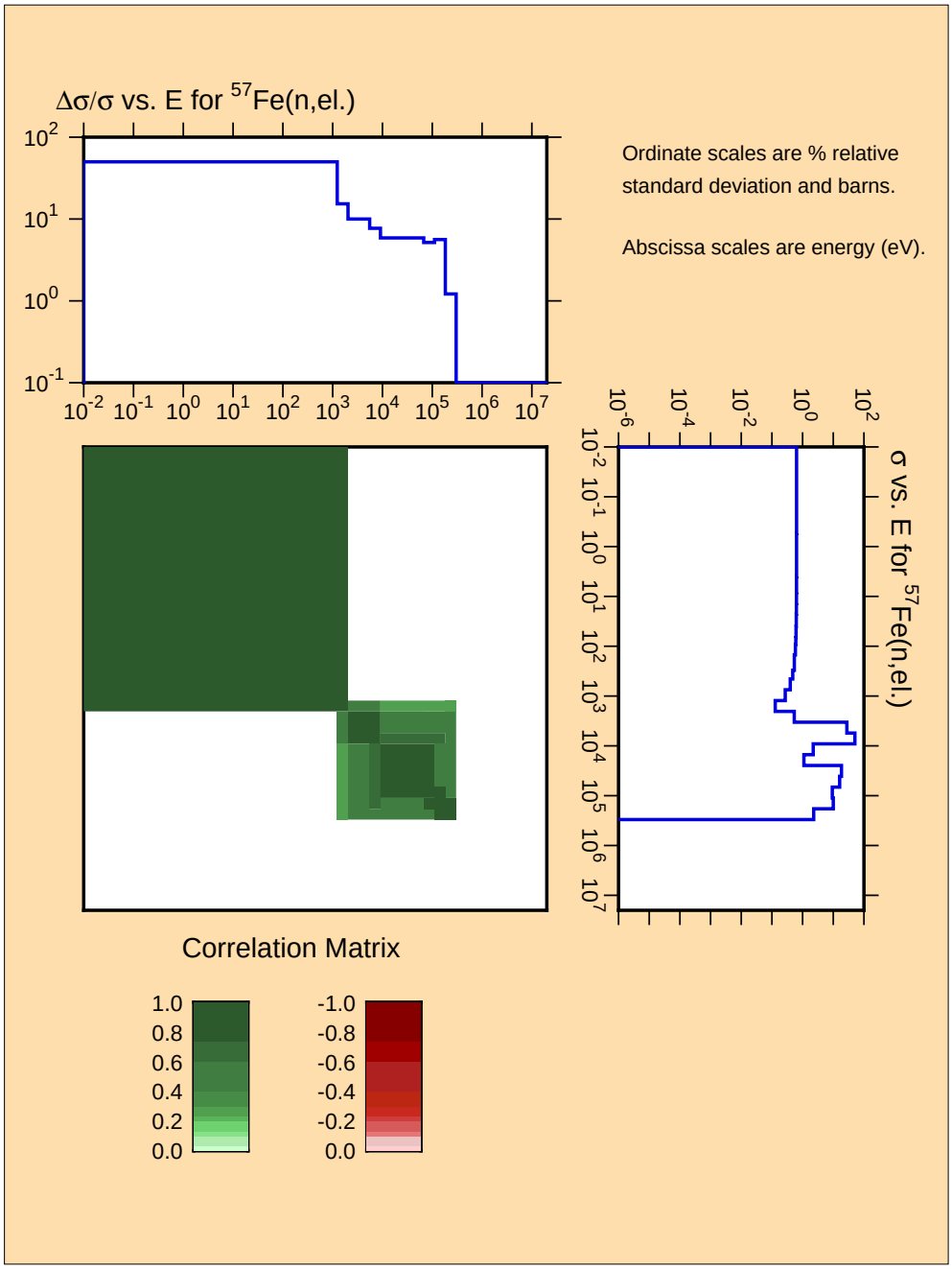

Figure 3.32: ^{57}Fe(n,el) covariances in the thermal and resonance region for the uniformly adopted value of level-level and bin-bin correlation coefficients, corr = 0.5.

3.6 ^{60}Ni evaluation

Evaluation is performed in several consecutive steps. We start with inspecting capture and elastic scattering cross sections in ENDF/B-VII.0 library. Then, we identify the proper energy binning for average cross sections, compute uncertainties for the average cross sections in these energy bins, and finally combine the bins into covariance matrix. Details can be seen on subsequent plots.

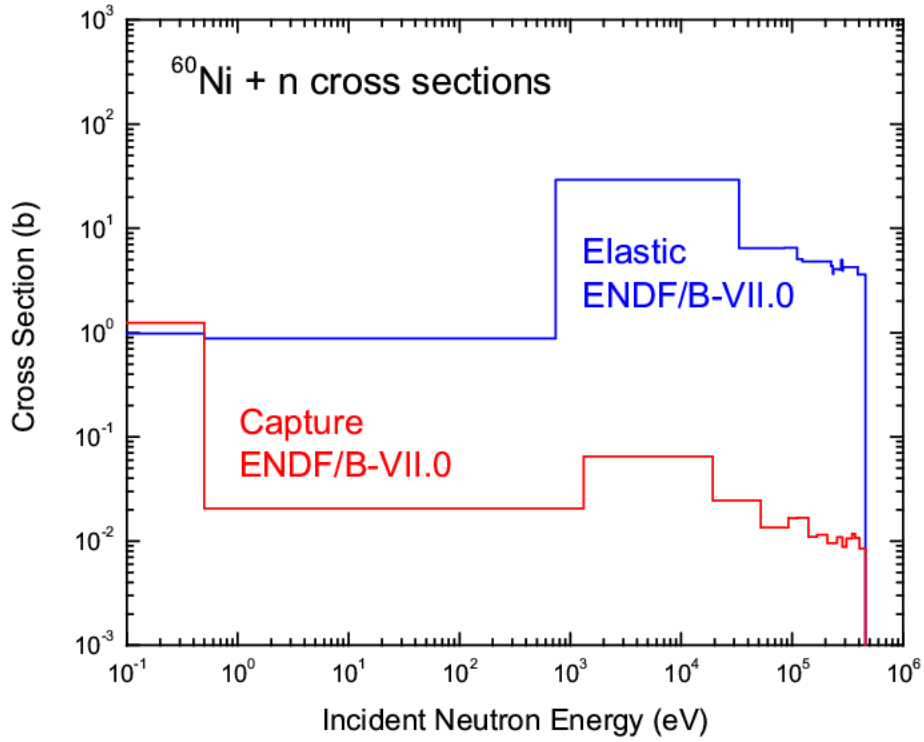

Figure 3.33: ^{60}Ni(n,γ) and (n,el) average cross sections in the thermal and resonance region using resonance parameters from ENDF/B-VII.0 processed by NJOY.

3.6.1 Capture

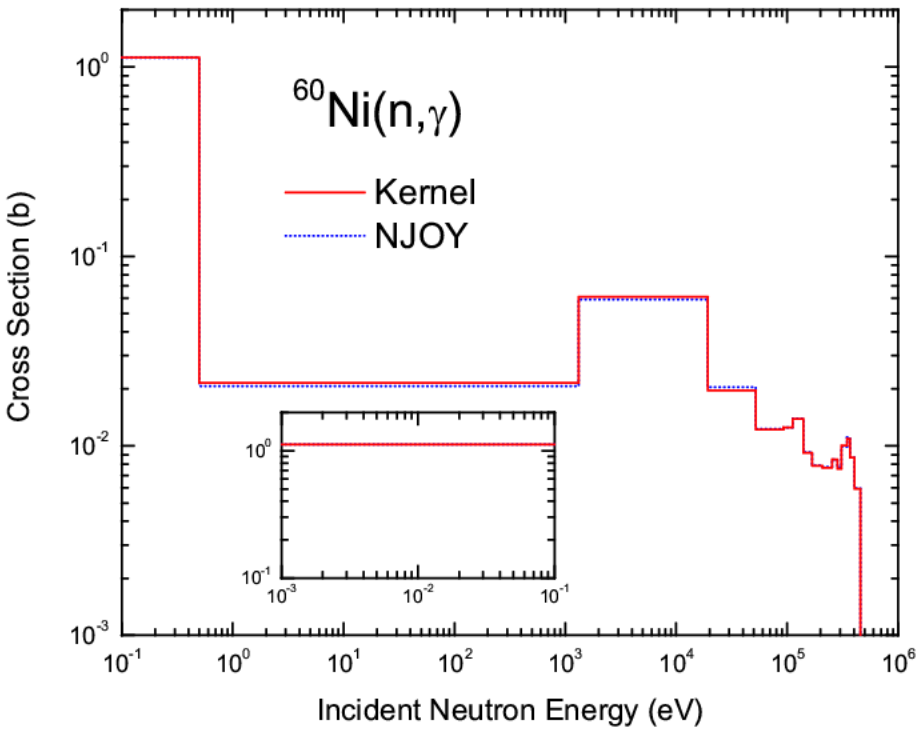

Figure 3.34: ^{60}Ni(n,γ) average cross sections using resonance parameters from Atlas. Compared are approximate values obtained by kernel formalism with correct values obtained by NJOY, demonstrating an excellent agreement. Shown in the insert is the thermal region.

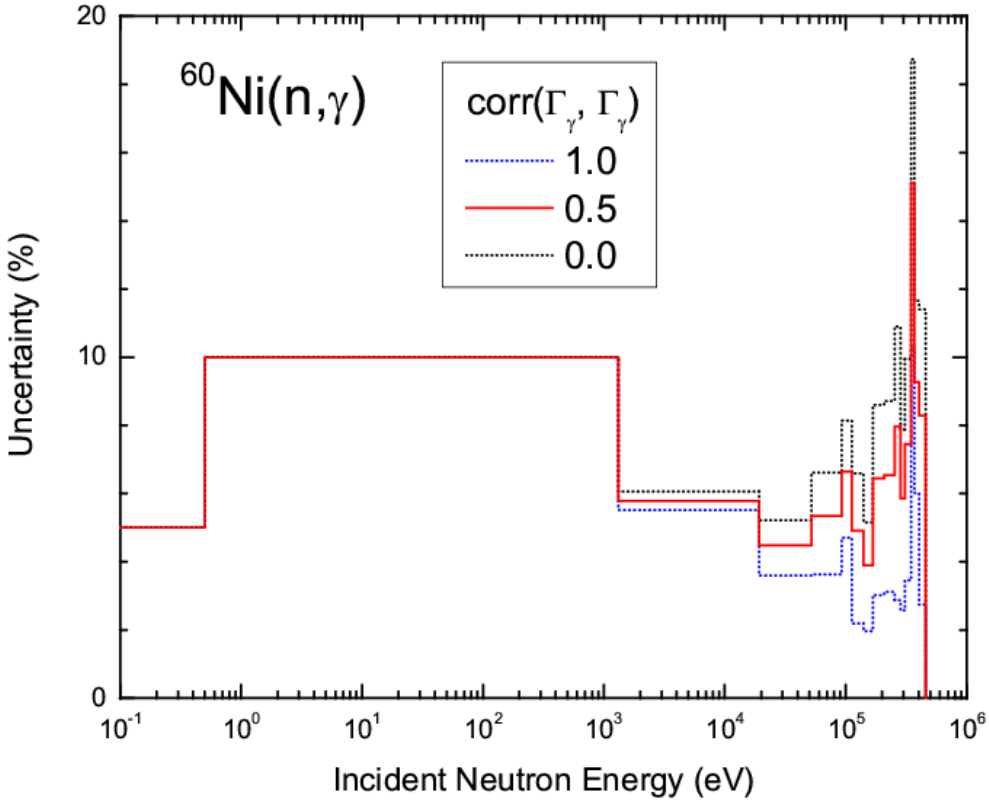

Figure 3.35: ^{60}Ni(n,γ) uncertainties for three scenarios of level-level correlation between radiative widths, corr(Γ_γ, Γ_γ) = 1.0, 0.5 and 0.0.

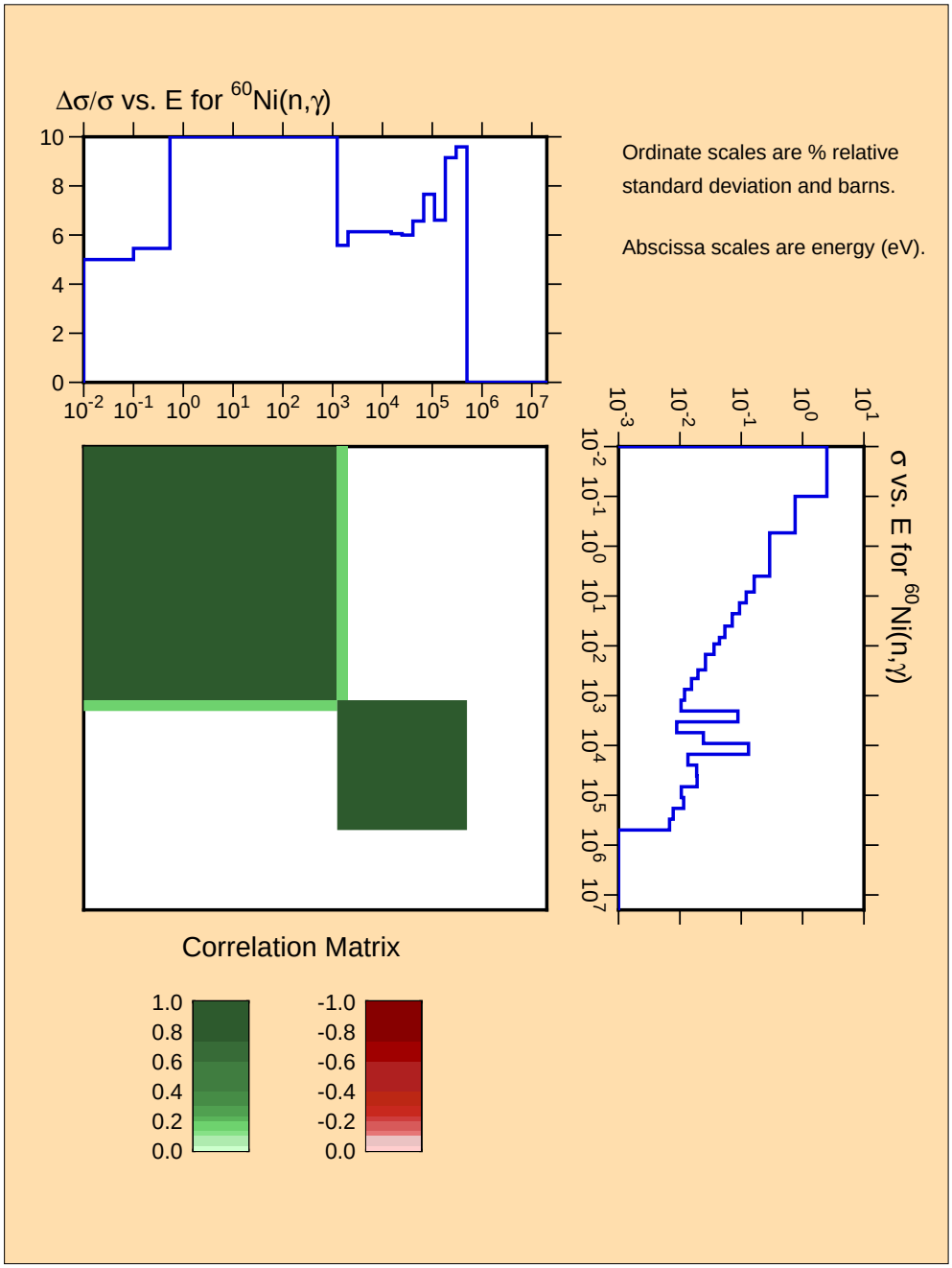

Figure 3.36: ^{60}Ni(n,γ) covariances in the thermal and resonance region for the level-level correlation coefficients adopted uniformly in the entire energy range corr = 0.5, while bin-bin corr = 1.0 was adopted in the final analysis. Shown are relative uncertainties in % (top), average cross sections in barns (right) and correlation matrix (bottom).

3.6.2 Elastic

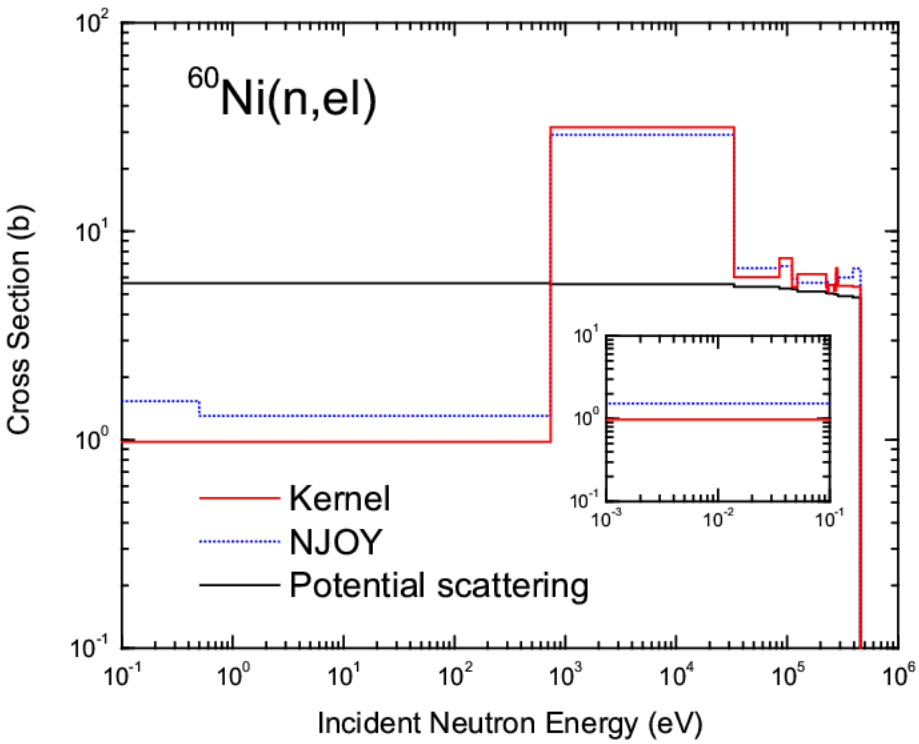

Figure 3.37: ^{60}Ni(n,el) average cross sections in the resonance region using resonance parameters from Atlas. Compared are approximate values obtained by kernel formalism with correct values obtained by NJOY. Shown in the insert is the thermal region. Potential scattering cross sections are shown explicitly, indicating dominant role of potential scattering at high energies.

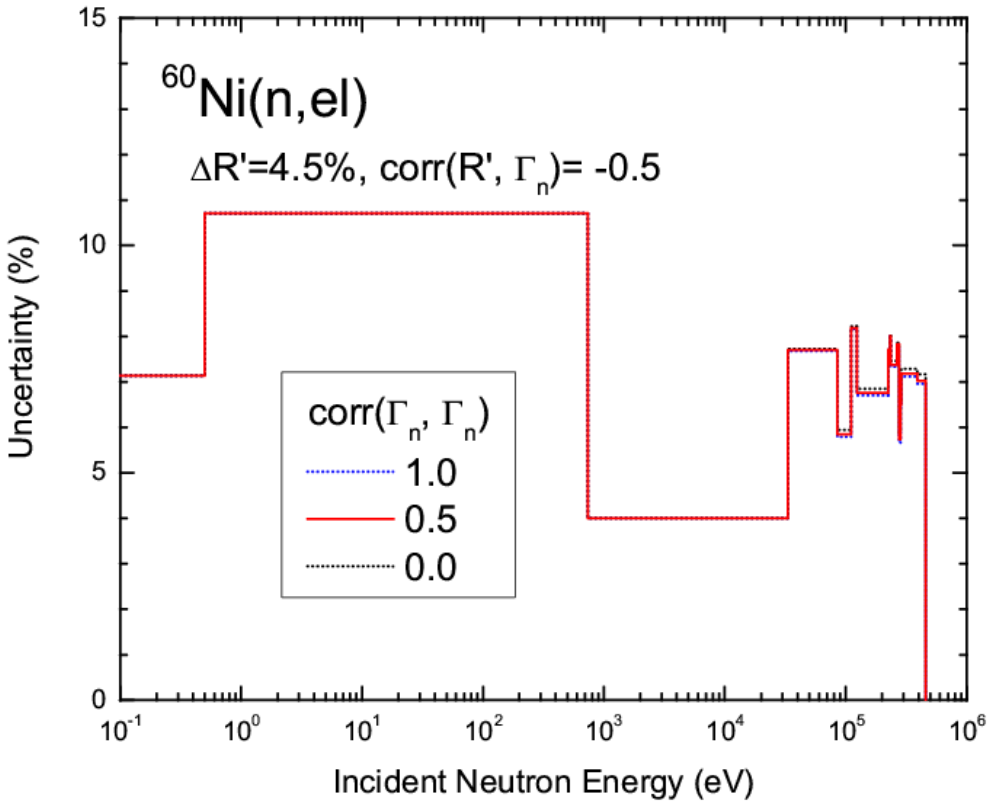

Figure 3.38: ^{60}Ni(n,el) uncertainties for three scenarios of level-level correlation between neutron widths, corr(Γ_n, Γ_n) = 1.0, 0.5 and 0.0. Assumed was scattering radius uncertainty $\Delta R'$ = 4.5% and default value of the correlation coefficient corr(R', Γ_n) = -0.5.

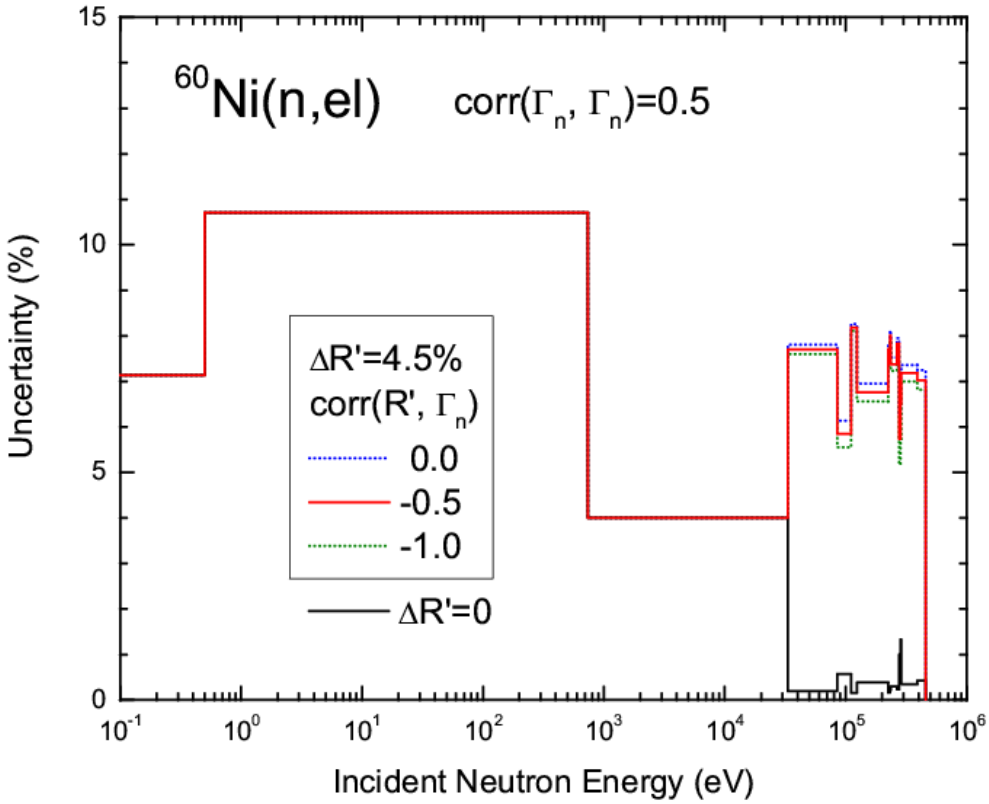

Figure 3.39: ^{60}Ni(n,el) uncertainties for three scenarios of corr(R', Γ_n) = 0.0, -0.5 and -1.0 assuming $\Delta R'$ = 4.5%. Shown for comparison are uncertainties assuming perfectly known scattering radius, $\Delta R'$ = 0, illustrating dominant impact of $\Delta R'$ on elastic scattering cross section uncertainties at high energies.

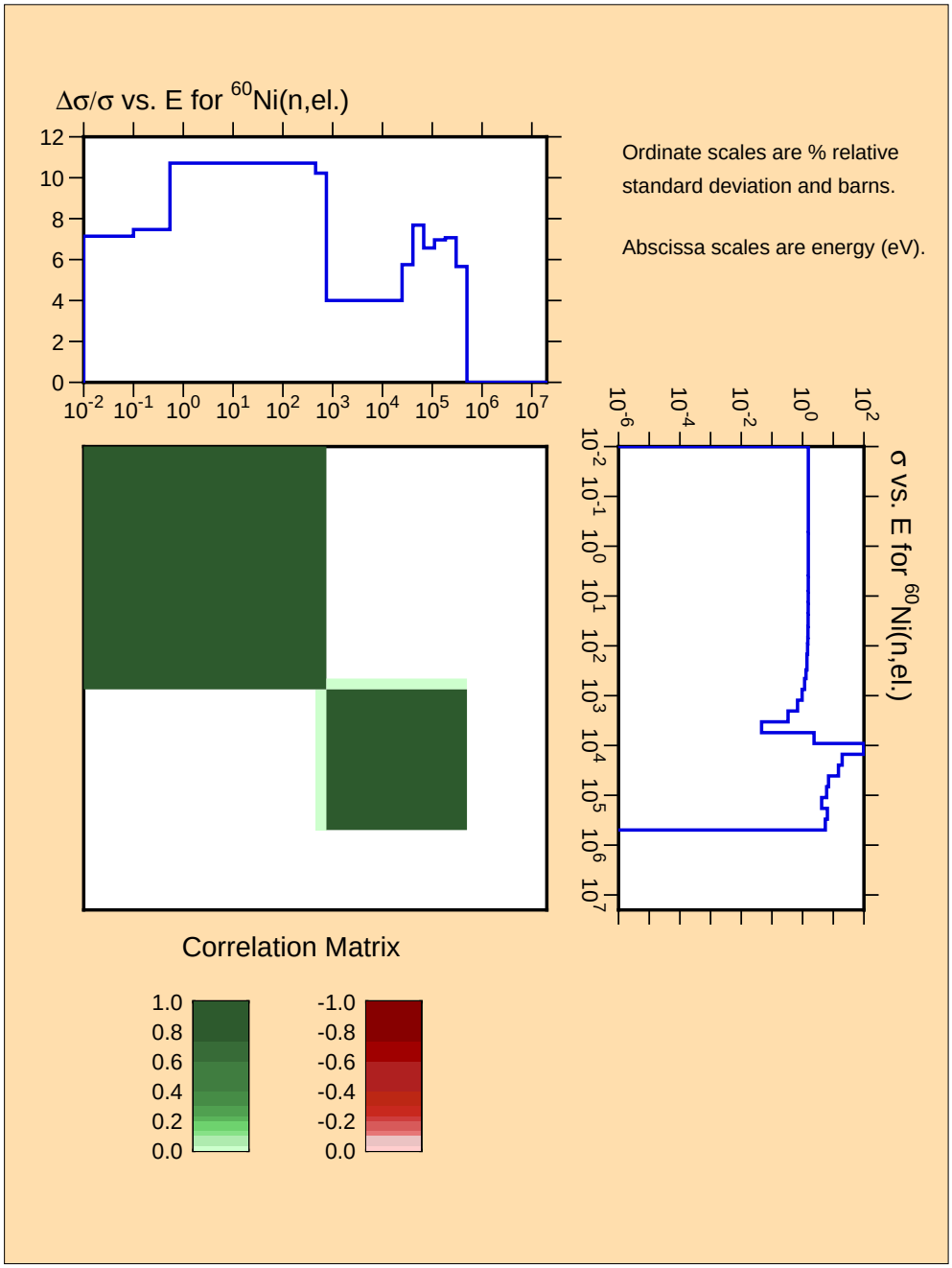

Figure 3.40: ^{60}Ni(n,el) covariances in the thermal and resonance region for the uniformly adopted value of level-level correlation coefficients corr = 0.5, while bin-bin corr = 1.0 was adopted in the final analysis.

Chapter 4

Quality assurance

Quality Assurance (QA) of covariances is important aspect of the evaluation process. Our QA procedures address formatting, mathematical properties of covariances matrices and plausibility of cross section uncertainties.

4.1 Compliance with ENDF-6 format

We used MF33 covariance format which was implemented in fairly simple and straightforward manner for all materials under discussion. Covariance matrices are supplied for capture and elastic scattering, they comply with the format as specified in the latest version of ENDF-6 Formats Manual [6].

4.2 Mathematical properties of covariance matrices

This QA test consists of three requirements:

- Symmetry. All our matrices are symmetric,

$$\mathrm{cov}(i, j) = \mathrm{cov}(j, i). \tag{4.1}$$

- Schwarz inequality. Correlation coefficients in each of our matrices are within -1.0 and +1.0 boundaries,

$$-1 \leq \mathrm{corr}(i, j) \leq 1. \tag{4.2}$$

- Positive-definiteness. Eigenvalues of our matrices should be either positive or at least semi-positive. This means that after diagonalizing a matrix all diagonal elements meet requirement

$$\mathrm{cov}(i, i) \geq 0. \tag{4.3}$$

  We note that the way how we constructed the matrices does not implicitly guarantee their positive-definitiveness. However, the matrices are fairly simple and the fix, if at all necessary, is relatively easy to do with small impact on final results.

4.3 Cross section uncertainties

There are no established procedures how to judge quality of cross section covariances. Probably the most sophisticated system is under development for AFCI applications [3] by the NNDC, its basic idea being inspection of covariances from several different perspectives. This includes integral perspective, where one compares own results with uncertainties of independently determined integral quantities (thermal, RI, Maxwellian average, Cf average). The second perspective is differential, where one analyzes dispersion of major evaluated libraries and performs comparison with differential data retrieved from EXFOR. The third perspective is testing against a set of criteria designed to check plausibility of uncertainties in broader energy groups.

In the present work we resorted to the following three tests. First, for capture we performed comparison with independent sources of information on integral quantities. For elastic scattering things are more complicated and we resorted to a comparison with independent estimate for the unresolved resonance region. As the third test we checked whether our uncertainties do not fall below certain acceptable limits, the goal being to avoid claims of unrealistic precision of cross sections.

4.3.1 Capture

We compared our results with three integral quantities: thermal values - comparison was made with data in Atlas adjusted for discrepancies with ENDF/B-VII.0 cross sections; resonance integrals - comparison was made with data in Atlas; 30-keV Maxwellian average - comparison was made with the uncertainties given in

Atlas and also in KADoNiS library [7] which is an independent database maintained by the nuclear astrophysics community. These three integral quantities effectively cover the energy range from the thermal point up to about 100-200 keV. This should be sufficient for AFCI applications, above about 100 keV capture cross sections are very small and hence of limited practical importance.

Summary of capture integral uncertainty testing for ^{50,53}Cr, ^{54,57}Fe and ^{60}Ni is given in Table 4.1. Our findings including recipes for possible fixes are as follows:

- In the thermal region our uncertainties either agree with Atlas or are more conservative since we accounted for discrepancies with cross sections in ENDF/B-VII.0 library. In all instances our covariances perform well.

- For capture resonance integrals things are more complicated. Thus, for three materials, ^{54,57}Fe and ^{60}Ni, performance of our results is good. For ^{50,53}Cr, however, our uncertainties differ considerably from recommended uncertainties obtained according to Eq. (3.2).

  We note that fixing resonance integral uncertainty for ^{50,53}Cr would be possible by the following consideration. RI_γ can be approximated as

  $$RI_\gamma = \int_{0.5\ eV}^{20MeV} \frac{1}{E}\sigma_\gamma(E)dE \approx \int_{0.5\ eV}^{1\ keV} \frac{1}{E}\sigma_\gamma(E)dE\,. \tag{4.4}$$

  This approximation takes into account 1/E weighting function as well as strong decline of capture cross sections for all materials under discussion meaning that one can neglect contributions from E $\gtrsim$ 1 keV. If according to Eq. (2.1) one would adopt

  $$\Delta\sigma_\gamma(E) = \Delta RI_\gamma \quad \text{for } 0.5\ eV < E \lesssim 1\ keV, \tag{4.5}$$

  then good agreement with capture integral resonance uncertainty could be achieved.

- 30-keV Maxwellian averages offer a good possibility to check our results effectively in the energy range from about 5 keV to 200 keV. One can see that even though the agreement is not unreasonable, our results look a bit too optimistic. It is not clear how to fix these discrepancies, one possibility would be to enhance radiative width uncertainties in Atlas.

Table 4.1: Capture integral quantities (thermal cross sections, $\sigma_\gamma(E_{th})$; resonance integrals, RI_γ; 30-keV Maxwellian averages, MACS) and their uncertainties for 5 minor structural materials. Shown are values in ENDF/B-VII.0 and Atlas, for MACS also in KADoNis [7]. Recommended uncertainties were obtained following Eqs. (3.1) and (3.2).

Nuc-	Quantity	VII.0	A t l a s		Rec.	Present	Performance
leus		b	b	%	%	%	and possible fix
^{50}Cr	$\sigma_\gamma(E_{th})$	15.9	15.4±0.2	1.3	1.9	2.0	Performance good
	RI_γ	7.48	11.7±0.2	1.7	22	3.5	Fix possible via thermal
	MACS	37.8mb	49±12mb	24	24	7.6	Fix not easy
	KADoNiS	37.8mb	49±13mb	26	26	7.6	Fix not easy
^{53}Cr	$\sigma_\gamma(E_{th})$	18.1	18.6±0.6	3.2	3.2	3.3	Good; see also ENDF/A[a)]
	RI_γ	8.43	12.3[c]	-	19	6.1	Fix possible via thermal
	MACS	31.4mb	54±9.4mb	17	26	13	Fix not easy
	KADoNiS	31.4mb	58±10mb	17	29	13	Fix not easy
^{54}Fe	$\sigma_\gamma(E_{th})$	2.25	2.25±0.18	8.0	8.0	8.0	Performance good
	RI_γ	1.20	1.27±0.10[c]	7.9	8.1	8.0	Performance good
	MACS	21.6mb	34±3mb	9	22	9.6	Fix not easy
	KADoNiS	21.6mb	29.6±1.3mb	4.4	15	9.6	Performance reasonable
^{57}Fe	$\sigma_\gamma(E_{th})$	2.43	2.48±0.30	12	12	12	Performance good
	RI_γ	1.45	1.52±0.15[c]	9.9	10	10	Performance good
	MACS	28.5mb	-	-	-	14.4	
	KADoNiS	28.5mb	40±4mb	10	17	14.4	Performance good
^{60}Ni	$\sigma_\gamma(E_{th})$	2.76	2.50±0.06	2.4	5.1	5.0	Performance good
	RI_γ	1.40	1.40±0.20[c]	14	14	14	Good; see also ENDF/A[b)]
	MACS	28.3mb	-	-	-	6.4	
	KADoNiS	28.3mb	29.9±0.7mb	2.3	2.7	6.4	Fix not easy

[a)] ^{53}Cr [9], retrieved from ENDF/A in July 2010: $\sigma_\gamma(E_{th})$ = 18.09±0.42b

[b)] ^{60}Ni [10], retrieved from ENDF/A in July 2010: RI_γ = 2.40±0.06b

[c)] Value in Atlas is computed.

4.3.2 Elastic scattering

For elastic scattering we resorted to a comparison of uncertainties for two energies as shown in Table 4.2. For thermal energies our results agree will with those in Atlas except for ^{57}Fe. This good agreement is not surprising and it is in line with our evaluation procedure adopted in the thermal region. Disagreement for ^{57}Fe is due to large discrepancy between thermal elastic cross section in ENDF/B-VII.0 (2.62 b) and Atlas (0.68 b).

Table 4.2: Uncertainties for elastic scattering cross sections for ^{52,53}Cr, ^{54,57}Fe and ^{60}Ni. Shown are thermal values and those at around 100 keV. Comparison is made between Mughabghab (thermal - Atlas, see also Table 3.2; 100 keV - new estimates [11]) and present results.

Nuclide	Energy	Mughabghab %	Present %	Comment
^{50}Cr	thermal	2.5	2.5	Good agreement
	100 keV	13.4	11	Good agreement
^{53}Cr	thermal	2.6	2.6	Good agreement
	100 keV	14.2	7.5	Modest agreement
^{54}Fe	thermal	4.6	4.6	Good agreement
	100 keV	14.6	5.3	Modest agreement
^{57}Fe	thermal	8.8	50	Large discrepancy with VII.0
	100 keV	9.8	6.1	Reasonable agreement
^{60}Ni	thermal	7.1	7.1	Good agreement
	100 keV	10.6	7.2	Reasonable agreement

As the second energy we show comparison at around 100 keV with independent estimate done most recently by Mughaghab [11]. He used expression for the unresolved resonance region which relates average total cross sections with the scattering radius R' and neutron s-wave and p-wave strength functions S_0 and S_1. Then, he carried out a least-squares fit to the total cross sections to derive these quantities as well as their uncertainties. Since at 100 keV capture cross section can

be neglected, uncertainty of elastic scattering cross section is fully determined by uncertainty of total cross section. One can see that the two approaches yield comparable results, though our uncertainties are systematically lower. This seems acceptable since our results are based on averaging of individual resonances around 100 keV rather than on averaging over the entire resonance region.

4.3.3 Minimal uncertainties

We adopted criterion that uncertainties in the 33-group representation should be larger than reasonable minimal values, which were set to 2%. We thus require

- $\Delta\sigma(n,\gamma) > 2\%$,
- $\Delta\sigma(n,el) > 2\%$.

These minimal values take into account the fact that to reach 2% precision in neutron cross section measurements is tough. Better precision has been achieved in determining the best established cross sections of neutron standards.

We checked all uncertainties and made sure that if precision better than 2% is claimed, then plausible explanation is available. This test produced warning only once, 1.88% for ^{50}Cr(n,γ) in the border between thermal and resonance region as artifact of processing. In the thermal region we adopted 2.0% value (1.3% from Atlas corrected for discrepancy with the thermal cross section in ENDF/B-VII.0); in the 1st resonance bin capture kernel is known also to about 2%. Since correlation between these two bins was estimated to be 0.5, quadratic summation gives a value smaller than 2%.

Chapter 5

Conclusions

We evaluated covariances for neutron capture and elastic scattering on ^{50,53}Cr, ^{54,57}Fe and ^{60}Ni in the resonance region which extends to hundreds keV for each of them. This work complements our earlier evaluation of three major structural materials, ^{50}Cr, ^{56}Fe and ^{58}Ni. Use was made of the recently developed covariance formalism based on kernel approximation along with data in the Atlas of Neutron Resonances. Covariances in the thermal region were directly deduced from experimental data and thus treated independently from the resonance region. Our results should serve as covariances for central cross section values in ENDF/B-VII.0 library. Processed 33-group data should be adopted by AFCI-2.0 covariance library.

Kernel approximation works very well for capture. All materials under discussion are almost pure scatterers, meaning that neutron widths are much larger than radiative widths, $\Gamma_n >> \Gamma_\gamma$. Therefore, capture covariances are essentially determined by radiative width uncertainties, $\Delta\Gamma_\gamma$ and they strongly depend on level-level correlations, corr($\Gamma_\gamma, \Gamma_\gamma$), which had to be estimated.

Kernel approximation for elastic scattering represents less robust approach. This is mostly due to interference effects. Fortunately, elastic cross sections at high energies are dominated by potential scattering and covariances are thus determined by scattering radius uncertainty, $\Delta R'$.

Our results were subject to QA checks, including compliance with ENDF-6 formatting, mathematical properties of covariance matrices and limited uncertainty testing. Uncertainties were tested against a few available integral quantities and against 2% minimal value.

Acknowledgments

The authors are grateful to Ramon Arcilla (BNL) for careful computation of uncertainties of integral quantities with the processing code NJOY. We would like to thank Mark Williams and Goran Arbanas (ORNL) for illuminating discussion on estimating uncertainties of discrepant data. One of us (YSC) is grateful to the NNDC for warm hospitality extended to him during the course of this work.

This work has been performed under AFCI covariance data project sponsored by DOE-NE. It was also part of ARRA project of developing neutron cross section covariances for ENDF/B-VII library sponsored by DOE-SC. This sponsorhip is gratefully acknowledged. Brookhaven National Laboratory is sponsored by the Office of Nuclear Physics, Office of Science of the U.S. Department of Energy under Contract No. DE-AC02-98CH10886 with Brookhaven Science Associates, LLC.

Bibliography

[1] P. Obložinský, Y.-S. Cho, C. Mattoon, S.F. Mughabghab, "Neutron cross section covariances in the resonance region: ^{52}Cr, ^{56}Fe and ^{58}Ni", Brookhaven National Laboratory Report, Report BNL-93903-2010 (August 2010).

[2] P. Obložinský, Y.-S. Cho, C. Mattoon, S.F. Mughabghab, "Formalism for neutron cross section covariances in the resonance region using kernel approximation", Brookhaven National Laboratory Report, Report BNL-91287-2010 (April 2010).

[3] P. Obložinský, C. Mattoon, M. Herman, S.F. Mughabghab, M. Pigni, P. Talou, G. Hale, A.C. Kahler, T. Kawano, R. Little, P. Young, "Progress on Nuclear Data Covariances: AFCI-1.2 Covariance Library", Brookhaven National Laboratory, Report BNL-90897-2009 (September 2009).

[4] S.F. Mughabghab, "Atlas of Neutron Resonances: Thermal Cross Sections and Resonance Parameters", Elsevier Publisher, Amsterdam, 2006.

[5] R.C. Little *et al*, "Low-fidelity Covariance Project", Nuclear Data Sheets **109** (2008) 2828.

[6] M. Herman and A. Trkov (editors), "ENDF-6 Formats Manual: Data Formats and Procedures for the Evaluated Nuclear Data File ENDF/B-VI and ENDF/B-VII", Brookhaven National Laboratory, Report BNL-90365-2009 (CSEWG Document ENDF-102), June 2009, p. 317.

[7] "KADoNiS, Karlsruhe Astrophysical Database of Nucleosynthesis in Stars", www.kadonis.org, data retrieved in June 2010.

[8] M.L. Williams and G. Arbanas, ORNL, private communication to PO, August 2010.

[9] L. Leal, H. Derrien, K. Guber, G. Arbanas and D. Wiarda, "^{53}Cr ORNL Resonance Evaluation Including Covariance", September 2009, retrieved from ENDF/A in May 2010.

[10] H. Derrien, L. Leal, K. Guber, D. Wiarda and G. Arbanas, "Reevaluation of ^{60}Ni Resonance Parameters in the Energy Range Thermal to 810 keV", July 2009, retrieved from ENDF/A in May 2010.

[11] S.F. Mughabghab, "Uncertainty Treatment in the Unresolved Resonance Region", CSEWG Meeting, Santa Fe, November 2010, unpublished.